ARTICLE

BIK ubiquitination by the E3 ligase Cul5-ASB11 determines cell fate during cellular stress

Fei-Yun Chen[1,2], Min-Yu Huang[1,2], Yu-Min Lin[1,2], Chi-Huan Ho[1,2], Shu-Yu Lin[1], Hsin-Yi Chen[3], Mien-Chie Hung[4,5,6] , and Ruey-Hwa Chen[1,2]

The BH3-only pro-apoptotic protein BIK is regulated by the ubiquitin–proteasome system. However, the mechanism of this regulation and its physiological functions remain elusive. Here, we identify Cul5-ASB11 as the E3 ligase targeting BIK for ubiquitination and degradation. ER stress leads to the activation of ASB11 by XBP1s during the adaptive phase of the unfolded protein response, which stimulates BIK ubiquitination, interaction with p97/VCP, and proteolysis. This mechanism of BIK degradation contributes to ER stress adaptation by promoting cell survival. Conversely, genotoxic agents down-regulate this IRE1α–XBP1s–ASB11 axis and stabilize BIK, which contributes in part to the apoptotic response to DNA damage. We show that blockade of this BIK degradation pathway by an IRE1α inhibitor can stabilize a BIK active mutant and increase its anti-tumor activity. Our study reveals that different cellular stresses regulate BIK ubiquitination by ASB11 in opposing directions, which determines whether or not cells survive, and that blocking BIK degradation has the potential to be used as an anti-cancer strategy.

Introduction

Regulation of cell death is crucial for normal cell physiology, tissue homeostasis, and development. The Bcl-2 family determines the commitment of cells to apoptotic death and consists of three subgroups: the pro-survival Bcl-2–like proteins, the multidomain pro-apoptotic BAX/BAK proteins, and the pro-apoptotic BH3-only proteins. The BH3-only proteins function at the apex of the Bcl-2 family–controlled apoptotic pathway and activate BAX/BAK through two distinct mechanisms (Letai et al., 2002; Chen et al., 2005; Kuwana et al., 2005; Willis et al., 2007). In the direct activation mechanism, certain BH3-only proteins, such as BIM and tBID, bind BAX/BAK transiently to trigger their oligomerization at the outer mitochondrial membrane, thereby inducing cytochrome C release for apoptosis induction. However, most of the BH3-only proteins act through an indirect mechanism by binding to the pro-survival Bcl-2 proteins, thereby preventing them from neutralizing BAX/BAK.

Consistent with the function of BH3-only proteins as the fulcrum of the Bcl-2 family–governed apoptotic pathway, their expression and activity are tightly regulated under various physiological and stressed conditions. For instance, PUMA and NOXA are transcriptionally up-regulated by p53 under DNA damage (Oda et al., 2000; Nakano and Vousden, 2001), whereas

BIM is transcriptionally induced by CHOP during ER stress (Puthalakath et al., 2007). In addition to being regulated at the transcriptional level, BH3-only proteins also undergo various posttranslational modifications. For instance, BAD and BIM are negatively regulated by Akt- and ERK-induced phosphorylation, respectively (del Peso et al., 1997; Ewings et al., 2007). Ubiquitin-mediated proteolysis is another mechanism to regulate the abundance of BH3-only proteins, and BIM is the most well-studied member undergoing such a mode of regulation. BIM is ubiquitinated by the SCF-βTRCP complex upon phosphorylation by extracellular signal-regulated kinase (ERK)–ribosomal S6 kinase (RSK) cascade in the G1/S phase (Dehan et al., 2009) and by APC[cdc20] during mitosis (Wan et al., 2014). Regulation of these ubiquitination pathways could have an influence on the sensitivity of cancer cells to anti-tumor agents.

BIK is the founding member of BH3-only proteins (Boyd et al., 1995). In addition to the BH3 domain, BIK contains a transmembrane domain at its C-terminus and is mainly localized to the membrane of ER (Germain et al., 2005). BIK facilitates the release of ER Ca^{2+} store in a BAX/BAK-dependent manner (Mathai et al., 2005). The released Ca^{2+} is transferred to mitochondria via ER–mitochondria contact sites, thereby

---

[1]Institute of Biological Chemistry, Academia Sinica, Taipei, Taiwan;   [2]Institute of Biochemical Sciences, College of Life Science, National Taiwan University, Taipei, Taiwan; [3]Graduate Institute of Cancer Molecular Biology and Drug Discovery, College of Medical Science and Technology, Taipei Medical University, Taipei, Taiwan;   [4]Department of Molecular and Cellular Oncology, The University of Texas MD Anderson Cancer Center, Houston, TX;   [5]Department of Biotechnology, Asia University, Taichung, Taiwan; [6]Center for Molecular Medicine and Graduate Institute of Cancer Biology, China Medical University, Taichung, Taiwan.

Correspondence to Ruey-Hwa Chen: rhchen@gate.sinica.edu.tw.

activating dynamin-related GTPase DRP1 for mitochondrial cristae remodeling and cytochrome C release (Prudent and McBride, 2017). BIK also increases ER-associated BAK and disrupts the interaction between Bcl-2 and inositol-1,4,5-triphosphate receptor, both of which contribute to the Ca^{2+} release from ER (Mebratu et al., 2017). Similar to several other BH3-only members, BIK is transcriptionally up-regulated by p53 and E2F (Mathai et al., 2002; Real et al., 2006). In addition, BIK is a labile protein and can be stabilized by proteasome inhibitor (Zhu et al., 2005; Li et al., 2008). Although such a finding indicates that BIK is regulated by ubiquitination, the ubiquitin ligase responsible for this regulation has not been identified.

The unfolded protein response (UPR) is a cellular adaptive program aimed at restoring ER homeostasis under various ER-stressed conditions. UPR is activated by the accumulation of misfolded proteins in the ER lumen and is mediated by three ER membrane–localized stress-sensing proteins, including inositol-requiring enzyme 1 (IRE1), activating transcription factor 6 (ATF6), and protein kinase RNA-like ER kinase (PERK; Hetz et al., 2011). The outcome of UPR can be pro-survival or pro-apoptosis depending on the strength and duration of ER stress (Maurel et al., 2015). Under transient and mild stress conditions, UPR promotes cell survival by increasing protein folding or degradation and inhibiting protein synthesis. Under chronic ER stress, UPR facilitates apoptosis by altering the expression and/or activity of a set of pro-apoptotic regulators, including several Bcl-2 family proteins (Rodriguez et al., 2011). However, it remains unclear whether UPR can regulate Bcl-2 family proteins to promote cell survival during the adaptive phase. Furthermore, the mechanisms by which UPR switches from the adaptive to apoptotic phase have not been completely understood.

In this study, we identify Cul5-ASB11 as a ubiquitin ligase targeting BIK for ubiquitination and proteasomal degradation. Under ER stress, *ASB11* is transcriptionally activated by XBP1s, an effector of IRE1α. In contrast, DNA damage–induced p53 downregulates IRE1α to repress ASB11. Consequently, BIK ubiquitination and degradation are enhanced by ER stress and reduced by DNA damage, thereby oppositely regulating cell life/death decisions in the two stressed conditions. We also show that targeting the BIK degradation pathway in combination with the administration of an active BIK mutant could offer an effective anti-cancer strategy.

Results

Identification of Cul5-ASB11 as a BIK ubiquitin ligase
To identify ubiquitin ligase for BIK, we focused on Cullin-RING ubiquitin ligases (CRLs), which comprise the largest ubiquitin ligase family (Petroski and Deshaies, 2005). By using a dominant-negative (DN) mutant of each Cullin, we found that Cul2 and Cul5 mutants elevated the expression of BIK protein, but not *BIK* mRNA (Fig. 1 A and Fig. S1 A). Since DN mutants of Cul2 and Cul5 are promiscuous due to the sharing of ElonginB/C subunits by the two CRL complexes, we further validated the role of Cul2 and Cul5 using the knockdown approach. Remarkably, BIK expression was up-regulated by two independent Cul5 shRNAs, and this effect correlated with knockdown efficiency

(Fig. 1 B). However, Cul2 knockdown could not elevate BIK expression. These findings support an effect of CRL5 on BIK regulation. The CRL5 complex contains ROC2, Cul5, ElonginB, ElonginC, and one of many substrate adaptors with a suppressor of cytokines signalling (SOCS) box (Lydeard et al., 2013). To identify the Cul5 substrate adaptor responsible for BIK regulation, we expressed each of the 39 Cul5 substrate adaptors and tested their interaction with endogenous BIK by immunoprecipitation. This analysis identified ANKRD9, ASB11, and ASB17 as BIK-interacting proteins (Fig. S1 B). Among them, only ASB11 could potentiate BIK ubiquitination when expressed in vivo (Fig. S1 C). Similar to BIK, ASB11 is an ER-residing protein (Andresen et al., 2014). Immunoprecipitation analysis demonstrated the interaction of endogenous ASB11 with endogenous BIK in vivo and a direct interaction between purified ASB11 and BIK in vitro (Fig. 1, C and D). Furthermore, ASB11 knockdown impaired the in vivo interaction of BIK with Cul5 (Fig. S1 D). These findings are consistent with the adaptor role of ASB11 in recruiting BIK to the CRL5 complex. Similar to other Cul5 substrate adaptors, ASB11 possesses a SOCS box for binding Cul5 and ElonginB/C (Sartori da Silva et al., 2010; Andresen et al., 2014). We found that deletion of the SOCS box abolished the capability of ASB11 to promote BIK ubiquitination (Fig. 1 E). In addition, depletion of ASB11 in both 293T and H1299 cells reduced BIK ubiquitination (Fig. 1 F and Fig. S1 E). As to the ubiquitin chain type, ASB11 promoted BIK K48 ubiquitination (Fig. 1 G). In the in vitro ubiquitination assay, BIK ubiquitination was readily detected in the reaction supplemented with a full Cul5-ASB11 complex, including ROC2, Cul5, ElonginB, ElonginC, and ASB11 (Fig. 1 H). Together, our results support that Cul5-ASB11 is a direct and physiologically relevant ubiquitin ligase for BIK.

ASB11 promotes BIK proteasomal degradation
Next, we determined the consequence of BIK ubiquitination mediated by Cul5-ASB11. Overexpression of ASB11, but not its SOCS box deletion mutant, decreased the BIK protein level (Fig. 2 A). This effect of ASB11 was reversed by treatment of cells with the proteasome inhibitor MG132 (Fig. 2 B). Using a cyclo-heximide chase assay, we found that ASB11 overexpression increased BIK protein turnover (Fig. 2 C). In the reciprocal set of experiments, ASB11 knockdown in both 293T and H1299 cells elevated the BIK protein level (Fig. 2 D). Furthermore, ASB11 depletion increased BIK protein stability (Fig. 2 E). These findings indicate that ASB11-mediated BIK ubiquitination promotes its proteasomal degradation.

ASB11 is a transcriptional target of XBP1s
BH3-only proteins are usually regulated by various cellular stress signals. We investigated whether ASB11-mediated BIK ubiquitination could be regulated under cellular stress conditions. Remarkably, tunicamycin, which inhibits glycosylation to cause ER stress, up-regulated the expression of *ASB11* mRNA in multiple cell systems, including 293T, MDA-MB157, and MDA-MB468 cells (Fig. 3 A and Fig. S2 A). A similar up-regulation of *ASB11* mRNA was observed by another ER stressor, the calcium pump inhibitor thapsigargin (Fig. 3 A). Tunicamycin and thapsigargin also increased ASB11 protein levels (Fig. 3 B). To dissect
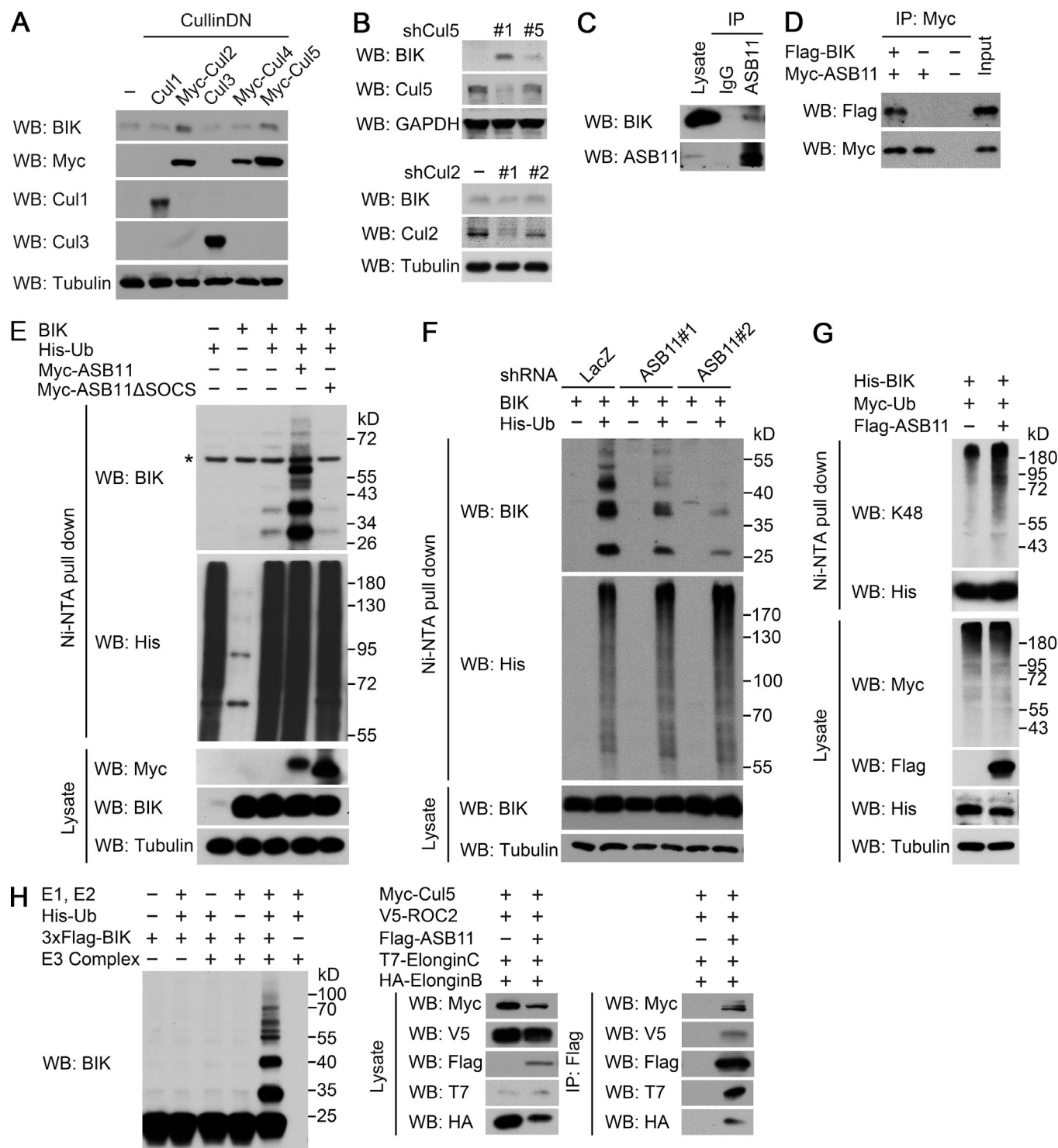
Chen et al.
BIK degradation in controlling stress responses

Journal of Cell Biology   3003
https://doi.org/10.1083/jcb.201901156

Figure 1. **Cul5^ASB11 targets BIK for ubiquitination. (A and B)** Western blot (WB) analysis of endogenous BIK expression in 293T cells transiently transfected with the indicated Cullin DN mutants (A) or transduced with lentivirus carrying the indicated shRNAs (B). **(C)** Immunoprecipitation (IP) analysis of the interaction between endogenous ASB11 and endogenous BIK in 293T cells. **(D)** In vitro interaction of ASB11 with BIK. Purified ASB11 bound on anti-Myc beads was incubated with BIK separately purified by and eluted from anti-Flag beads. The bound proteins were analyzed by Western blot. **(E)** Analysis of BIK ubiquitination in 293T cells transfected with the indicted constructs. The ubiquitinated proteins were pulled down under denaturing conditions by Ni-NTA agarose and analyzed by Western blot. The asterisk denotes a nonspecific band. **(F)** Analysis of BIK ubiquitination in 293T cells stably expressing control or ASB11 shRNA and transfected with the indicated constructs. The knockdown efficiencies of ASB11 shRNAs are shown in Fig. 2 D. **(G)** Analysis of BIK K48 ubiquitination in 293T cells transfected with the indicated constructs. BIK was precipitated from cell lysate under denaturing conditions by Ni-NTA agarose and analyzed by Western blot with K48 polyubiquitin chain–specific antibody. **(H)** In vitro ubiquitination assay for BIK. Flag-BIK purified from 293T cells was incubated with E1, E2, His-ubiquitin, and/or ASB11-based Cul5 complex purified from transfected cells. The integrity of the input E3 ligase complex is shown on the right.
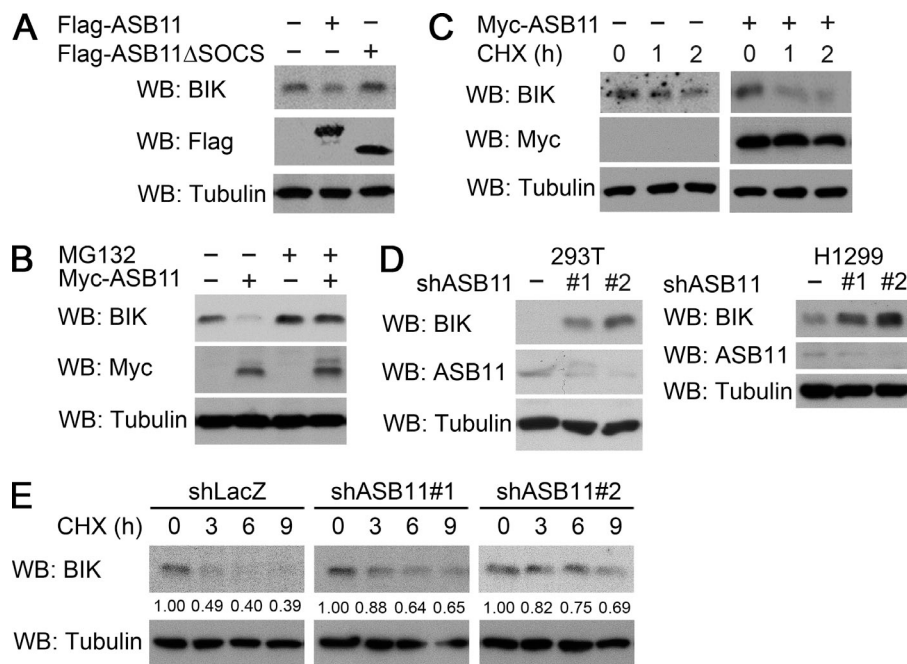
Chen et al.
BIK degradation in controlling stress responses

Journal of Cell Biology 3004
https://doi.org/10.1083/jcb.201901156

Figure 2. **ASB11 promotes BIK proteasomal degradation. (A)** Western blot (WB) analysis of endogenous BIK in 293T cells transfected with the indicated ASB11 constructs. **(B and C)** Western blot analysis of BIK levels in 293T cells transfected with ASB11 and treated with MG132 for 16 h or cycloheximide for the indicated time points. **(D)** Western blot analysis of BIK levels in the indicated cells stably expressing control or ASB11 shRNAs. **(E)** Western blot analysis of BIK in 293T derivatives as in D treated with cyclo-heximide for the indicated time points. The relative amounts of BIK are indicated by assigning the values from untreated cells as 1.

the molecular mechanism through which ER stress induces ASB11, we determined which of the three UPR branches is responsible for this effect. Blockage of the IRE1α–XBP1 axis by XBP1 depletion greatly suppressed tunicamycin-induced *ASB11* mRNA expression, whereas ATF6 or PERK knockdown showed an opposite effect (Fig. 3 C and Fig. S2 B). In response to ER stress, *XBP1* mRNA undergoes an IRE1α-dependent unconventional splicing to generate *XBP1s*, whose protein product functions as a transcription factor. Therefore, we set out to test whether *ASB11* is a transcriptional target of XBP1s. Overexpression of XBP1s greatly increased the *ASB11* mRNA level and the activity of a luciferase reporter driven by a 2-kb segment of the 5′ regulatory region of the *ASB11* gene (Fig. 3, D–F). Chromatin immunoprecipitation (ChIP) analysis with four pairs of primers (Fig. 3 E) revealed that endogenous XBP1s in tunicamycin-treated cells was specifically recruited to a region (−86 to −304) near the transcriptional start site of the *ASB11* gene (Fig. 3 G). However, no authentic XBP1s binding motif, such as UPRE, ERSE, ERSE-II, or AGCT core (Acosta-Alvear et al., 2007), could be found in this region. Instead, we identified an NF-Y binding motif in the position of −148 to −155. Since a previous report implicated the action of XBP1 on the NF-Y binding motif (Acosta-Alvear et al., 2007), we tested its importance. Luciferase reporter assay revealed that deletion of this NF-Y binding motif compromised XBP1s-induced *ASB11* promoter activity (Fig. 3 H), suggesting a cooperative action of these two transcription factors in the transcription of *ASB11*. In line with this notion, immunoprecipitation analysis demonstrated the interaction of endogenous XBP1s with each of the NF-Y complex components, NF-YA, NF-YB, and NF-YC (Fig. 3 I). Furthermore, depletion of NF-YB or NF-YC not only abrogated ER stress– or XBP1s-induced *ASB11* promoter activity, but completely blocked the binding of XBP1s to the *ASB11* promoter in tunicamycin-treated cells (Fig. 3, J–L). Thus, XBP1s is recruited to the *ASB11* promoter via NF-Y,

and this recruitment is crucial for the activation of *ASB11* transcription under ER stress.

ER stress induces a transient BIK degradation through the actions of Cul5-ASB11 and p97

Consistent with the elevated *ASB11* transcription under ER stress, tunicamycin and thapsigargin increased ASB11 protein expression and reduced BIK protein level in multiple cell lines (Fig. 4 A and Fig. S2 C). This effect of ER stress was reversed by pretreatment of cells with IRE1α inhibitor (Fig. S2 D). Of note, ASB11 up-regulation and BIK proteasomal degradation were observed transiently upon the induction of ER stress, which peaked at 12–16 h and then quickly returned to the levels seen in the unstressed cells (Fig. 4 B). This kinetics is consistent with the transient activation of the IRE1α–XBP1 axis reported previously (Lin et al., 2007; Chang et al., 2018). Within the ASB11 induction period, ER stress also increased the ubiquitination and turnover of endogenous BIK (Fig. 4, C and D). To corroborate that the reduced BIK level in ER-stressed conditions resulted from ASB11 up-regulation, we examined ASB11 knockdown cells. Indeed, ASB11 knockdown in multiple cell lines, including 293T, H1299, and MDA-MB157, abrogated tunicamycin-induced BIK down-regulation (Fig. 4 E and Fig. S2 E). Furthermore, tunicamycin-stimulated BIK ubiquitination and proteasomal degradation were all reversed by ASB11 knockdown (Fig. 4, F and G; and Fig. S2 F). In line with the critical role of XBP1 in ASB11 induction during ER stress, XBP1 knockdown blocked tunicamycin-induced BIK down-regulation and BIK ubiquitination (Fig. S2, G and H), whereas XBP1s overexpression increased ASB11 and decreased BIK expression (Fig. S2 I). Therefore, our study identifies a role of ER stress in promoting BIK ubiquitination and degradation through XBP1-induced ASB11 transcription.

BIK is an ER-residing transmembrane protein. We anticipated that extraction of ubiquitinated BIK from the ER membrane
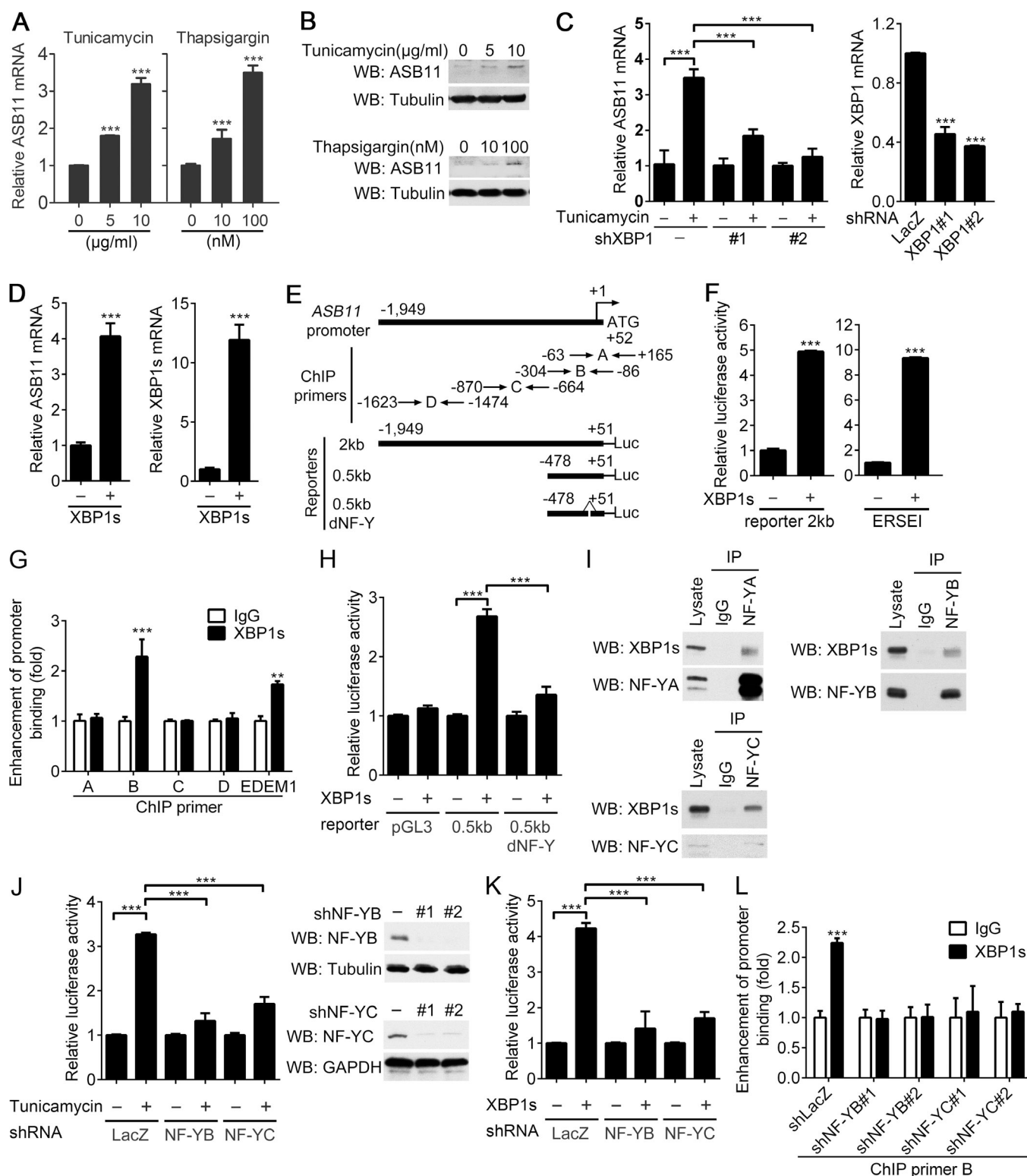
Chen et al.
BIK degradation in controlling stress responses

Journal of Cell Biology 3005
https://doi.org/10.1083/jcb.201901156

Figure 3. **ER stress induces *ASB11* transcription through the XBP1s–NF-Y complex. (A and C)** RT-qPCR analysis of the *ASB11* mRNA level in 293T cells (A) or 293T cells stably expressing control or XBP1 shRNAs (C) treated with tunicamycin or thapsigargin for 16 h. **(B)** Western blot (WB) analysis of ASB11 expression in 293T cells treated as in A. **(D)** RT-qPCR analysis of *ASB11* mRNA expression in 293T cells transfected with control vector or XBP1s. **(E)** Schematic representation of the 5′ regulatory region of the *ASB11* gene, the luciferase reporters, and the ChIP primers used in this study. **(F and H)** Luciferase reporter assays of 293T cells transfected with control or XBP1s expression construct together with the indicated reporter constructs. ERSEI reporter was used as a positive control. **(G and L)** Quantitative ChIP assays in 293T cells (G) or 293T derivatives (L) treated with 10 µg/ml tunicamycin for 4 h using control IgG or XBP1s antibody for immunoprecipitation and indicated sets of primers for qPCR. Primers encompassing the XBP1s binding region of the *EDEM1* promoter were used as a positive control. **(I)** Immunoprecipitation (IP) analysis of the interaction between endogenous XBP1s and each NF-Y complex component in 293T cells

Chen et al.
BIK degradation in controlling stress responses

Journal of Cell Biology 3006
https://doi.org/10.1083/jcb.201901156

treated with 10 µg/ml tunicamycin for 4 h. **(J and K)** Luciferase reporter assays of 293T cells stably expressing the indicated shRNAs and transfected with the 0.5-kb reporter construct together with XBP1s or treated with 10 µg/ml tunicamycin for 16 h. The knockdown efficiencies of the indicated shRNAs are shown on the right. Data in A, C, D, F–H, and J–L are mean ± SD; n = 3. P values were determined by t test (A and right panel in C, D, and F) or one-way ANOVA with Tukey's post hoc test (left panel in C, G, H, and J–L). **P < 0.01; ***P < 0.001.

would be critical for the subsequent degradation in proteasome. The AAA$^+$ ATPase p97, also known as the valosin-containing protein, is responsible for segregating numerous ubiquitinated proteins from organelle membranes to facilitate their proteasomal degradation (Meyer and Weihl, 2014; Avci and Lemberg, 2015; Ye et al., 2017). Moreover, p97, together with its cofactor UFD1L-NPL4 heterodimer, plays a crucial role in the degradation of ER-residing proteins under ER stress, a process called ER-associated degradation (ERAD; Ye et al., 2001). We thus determined the function of the p97–UFD1L–NPL4 complex in ER stress–induced BIK degradation. Remarkably, administration of the p97 inhibitor CB-5083 abrogated BIK down-regulation induced by ER stress or ASB11 overexpression (Fig. 4, H and I). Depletion of UFD1L or NPL4 also prevented BIK degradation in response to ER stress (Fig. 4, J and K). Furthermore, immunoprecipitation analysis revealed an increased interaction of p97 with ubiquitinated BIK in ER-stressed cells (Fig. 4 L). These findings support a role of the p97–UFD1L–NPL4 complex in governing proteasomal degradation of ubiquitinated BIK under ER-stressed conditions.

DNA damage induces p53-dependent BIK stabilization by suppressing the XBP1–ASB11 axis

In sharp contrast to ER-stressed conditions, genotoxic agents such as doxorubicin and 5-fluorouracil (5-FU) reduced *ASB11* mRNA levels in p53-proficient HCT116 cells, but not their p53-deficient counterparts (Fig. 5 A). Similarly, doxorubicin down-regulated *ASB11* mRNA in p53-transfected H1299 cells, but not in the parental, p53-deficient H1299 cells (Fig. S3 A). In line with these findings, doxorubicin and 5-FU down-regulated ASB11 protein and up-regulated BIK protein levels in a p53-dependent manner (Fig. 5 B). To determine whether protein stabilization attributes to the increased BIK level under DNA-damaged conditions, we evaluated BIK protein stability. In p53-proficient HCT116 cells, BIK protein turnover was decreased upon 5-FU treatment (Fig. 5 C, top panel). However, in ASB11-depleted HCT116 cells, BIK was readily stabilized, and DNA damage hardly induced a further increase in its stability (Fig. 5 C, second panel). These findings uncovered a DNA damage–induced and p53-dependent ASB11 down-regulation, leading to BIK stabilization.

Next, we sought to unravel the mechanism by which DNA damage reduces ASB11 expression. Since this effect is p53 dependent, we tested whether p53 regulates *ASB11* transcription. Consistent with this idea, *ASB11* mRNA expression was lower in p53-proficient HCT116 cells than in its p53-deficient counterpart (Fig. S3 B). Furthermore, p53 overexpression in H1299 cells decreased *ASB11* mRNA levels and promoter activity (Fig. S3, C and D). Nevertheless, we reasoned that p53 may not act on *ASB11* promoter directly, as a previous meta-analysis indicated that the transcriptional repression effect of p53 is mainly mediated by

indirect mechanisms (Fischer et al., 2014). Notably, p53 was reported to promote IRE1α degradation by interacting with the E3 ligase SYVN1/HRD1, even in unstressed cells (Namba et al., 2015). Consistently, we showed that doxorubicin and 5-FU reduced IRE1α levels and *XBP1* mRNA splicing through a p53-dependent manner (Fig. 5 D). To provide a causal link of p53-dependent IRE1α–XBP1 down-regulation to ASB11 down-regulation, we rescued XBP1s levels by overexpression. Indeed, XBP1s overexpression restored *ASB11* mRNA and protein expression and BIK ubiquitination in doxorubicin-treated cells (Fig. 5, E and F). Together, these data indicate that DNA damage–induced p53 represses the IRE1α–XBP1 axis, leading to ASB11 down-regulation and BIK stabilization.

Opposite regulations of ASB11-dependent BIK ubiquitination by ER stress and DNA damage govern the life/death cell fate

Having demonstrated that ER stress and DNA damage oppositely regulate *ASB11* transcription and BIK protein stability, we next determined the impact of these BIK regulations on cell life/death decisions. BIK knockdown decreased doxorubicin-induced apoptosis, indicating its physiological role in this cell death system (Fig. 6 A). Next, we interrogated the impact of DNA damage–induced ASB11 down-regulation and BIK stabilization on cell apoptosis by enforced expression of ASB11. Importantly, expression of ASB11, but not its SOCS box deletion mutant, attenuated apoptotic death in doxorubicin-treated cells (Fig. 6 B). ASB11 overexpression also diminished DNA damage–induced active caspase 3 and the cleaved form of poly ADP-ribose polymerase (PARP; Fig. 6 C). To substantiate that these anti-apoptotic effects of ASB11 are mediated by BIK degradation, we rescued BIK expression in ASB11-overexpressing cells. Indeed, BIK overexpression completely reversed the inhibitory effects of ASB11 overexpression on DNA damage–induced cell apoptosis, caspase 3 activation, and PARP cleavage (Fig. 6, D and E). These data support that DNA damage–induced ASB11 down-regulation and BIK stabilization contribute in part to the apoptotic paradigm of DNA damage responses.

The cellular response to ER stress exhibits a biphasic mode: adaptation at the early phase and apoptosis for persistent stress (Maurel et al., 2015). Since ASB11-mediated BIK degradation is induced specifically at the adaptive phase of UPR, we investigated whether this up-regulation of the ASB11–BIK axis could prevent cell death, thereby contributing in part to the stress adaptation. While the control cells showed a delayed apoptotic response, with no sign of apoptosis being observed at 12 and 24 h after tunicamycin treatment (i.e., the adaptive phase), ASB11 knockdown greatly accelerated the apoptotic phase, showing a significant apoptosis induction, caspase 3 activation, and PARP cleavage as early as 12 h (Fig. 7 A). Importantly, these effects of ASB11 knockdown were all reversed by BIK knockdown (Fig. 7, B and C). These findings support that ER stress–induced and
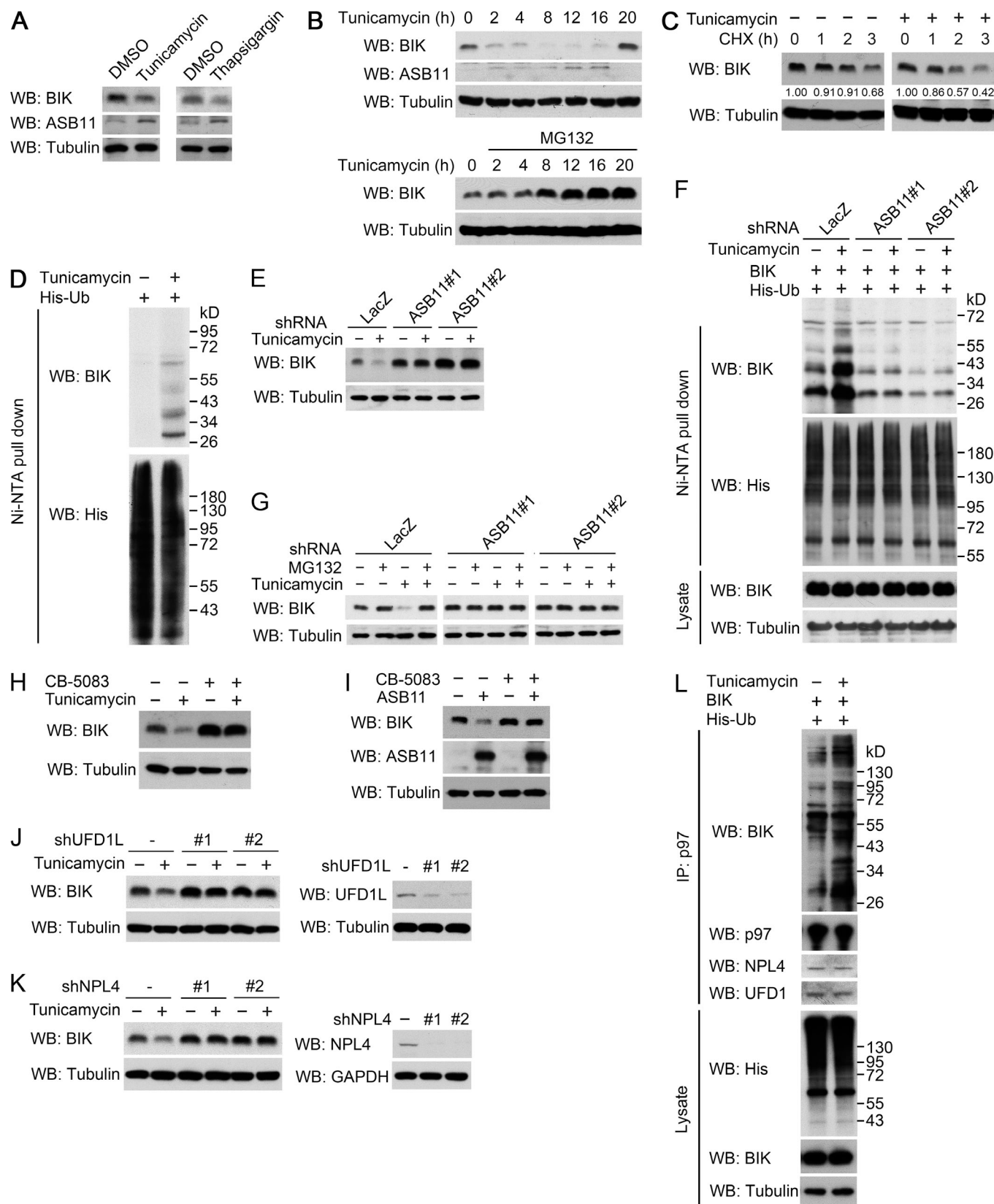
Chen et al.
BIK degradation in controlling stress responses

Journal of Cell Biology 3007
https://doi.org/10.1083/jcb.201901156

Figure 4. ER stress stimulates BIK ubiquitination and degradation through ASB11 and p97. (A) Western blot (WB) analysis of BIK and ASB11 levels in 293T cells treated with 10 µg/ml tunicamycin or 200 nM thapsigargin for 16 h. **(B)** Western blot analysis of BIK and ASB11 levels in 293T cells treated with tunicamycin (upper) or cotreated with tunicamycin and MG132 (lower) for the indicated time points. **(C)** Western blot analysis of BIK levels in 293T cells treated with 10 µg/ml tunicamycin for 12 h and then with 50 µg/ml cycloheximide (CHX) for the indicated time periods. The relative amounts of BIK are indicated by assigning the values from the initial time point as 1. **(D and F)** Analysis of endogenous (D) or exogenous (F) BIK ubiquitination in 293T cells (D) or 293T

derivatives as in Fig. 2 D (F) transfected with the indicated constructs and treated with tunicamycin. **(E)** Western blot analysis of 293T derivatives as in Fig. 2 D treated with 10 µg/ml tunicamycin for 16 h. **(G)** Western blot analysis of BIK levels in 293T derivatives cotreated with 10 µg/ml tunicamycin and MG132 for 16 h. **(H and I)** Western blot analysis of BIK expression in 293T cells cotreated with tunicamycin and 1 µM CB-5083 for 16 h (H) or transiently transfected with ASB11 and treated with CB-5803 for 16 h (I). **(J and K)** Western blot analysis of BIK expression in 293T cells stably expressing the indicated shRNAs and treated with 10 µg/ml tunicamycin for 16 h. The knockdown efficiency of each shRNA is shown on the right. **(L)** Immunoprecipitation (IP) analysis of p97 interaction with ubiquitinated BIK in 293T cells treated with 10 µg/ml tunicamycin for 16 h.

ASB11-mediated BIK degradation plays a pro-survival role to contribute to the adaptive phase of UPR. To further corroborate the effect of ASB11-dependent BIK ubiquitination on cell life/death fate under ER stress, we sought to generate an ASB11-resistant mutant of BIK. Mass spectrometry (MS) analysis of ubiquitinated BIK purified from cells expressing ubiquitin and ASB11 identified a ubiquitin modification on the residue K115 (Fig. S4 A). Disruption of the K115 residue decreased, but did not abolish, ASB11-induced BIK ubiquitination (Fig. 7 D). Replacement of both K115 and K160 residues with Arg (2KR mutant) completely abolished ASB11-dependent BIK ubiquitination and degradation (Fig. 7 D and Fig. S4 B) but did not affect its interaction with ASB11 (Fig. S4 C). We thus reexpressed wild-type BIK and BIK(2KR) mutant in BIK-depleted 293T cells. Of note, we chose the appropriate doses of two constructs so that the wild-type and mutant BIK proteins were expressed at comparable levels in unstressed conditions (Fig. 7 E). In contrast to wild-type BIK, the expression of BIK(2KR) was not affected by tunicamycin, consistent with the ASB11-resistant property of this protein. Consequently, BIK(2KR)-expressing cells showed an acceleration in the induction of cell apoptosis, caspase 3 activation, and PARP cleavage in response to tunicamycin treatment compared with cells expressing wild-type BIK (Fig. 7, F and G). Together, our findings indicate that induction of ASB11-mediated BIK ubiquitination and degradation represents a key mechanism by which the IRE1α–XBP1 axis prevents premature apoptosis to allow time for cell adaptation to ER stress.

Targeting the ASB11-dependent BIK degradation pathway enhances the anti-tumor effect of BIKDD

BIKDD, in which the Thr33 and Ser35 residues are replaced with Asp residues to mimic its phosphorylated form, has a higher affinity to the pro-survival Bcl-2 family proteins and thus represents an active mutant of BIK (Li et al., 2003). Due to its potent pro-apoptotic activity, tumor-selective expression of BIKDD has been demonstrated as an anti-tumor strategy in several preclinical models and can even eliminate tumor-initiating cells (Sher et al., 2009, 2011; Lang et al., 2011; Li et al., 2011; Xie et al., 2014). However, the labile feature of BIKDD has been a limitation. Notably, BIKDD also underwent ASB11-dependent and ER stress–induced ubiquitination and degradation (Fig. S5, A–D), and mutation of the K115 and K160 residues on BIKDD also abolished its ubiquitination and degradation induced by ASB11 (Fig. S5, E and F). Therefore, we reasoned that targeting this BIKDD degradation pathway would enhance its stability and anti-tumor efficacy. One way to inhibit ASB11-dependent BIKDD degradation is the administration of IRE1α inhibitor. As for the cancer type, we focused on triple-negative breast cancer (TNBC) for two reasons. First, TNBC is a highly aggressive disease with

limited treatment options. Second, BIKDD is particularly prone to degradation in TNBC due to the frequent up-regulation of the IRE1α–XBP1 axis (Chen et al., 2014), thus making its stabilization an important issue. We showed that the IRE1α inhibitor STF-083010 elevated BIKDD levels in multiple TNBC cell lines, including Hs578T, MDA-MB157, and MDA-MB468 (Fig. S5 G). Consequently, STF-083010 synergized with BIKDD in the killing of these TNBC cells (Fig. 8 A). The increased apoptotic effect of combinatory treatment was further supported by the increased level of cleaved PARP (Fig. 8 B). Importantly, in IRE1α knockdown cells or XBP1s-overexpressing cells, STF-083010 failed to enhance the cell-killing effect of BIKDD (Fig. S5, H and I), demonstrating the specificity of this agent. The killing effect of BIKDD on TNBC cells was also enhanced by combined administration of another IRE1α inhibitor, 4µ8C (Fig. S5 J). Besides the utilization of CMV-BIKDD, we tested the combinatory effect of IRE1α inhibitor together with VISA-BIKDD, which allows a selective expression of BIKDD in breast cancer cells (Lang et al., 2011). Importantly, the synergistic killing effect was observed by coadministration of VISA-BIKDD and STF-083010 (Fig. 8 C). Thus, our data support a beneficial effect of combinatory application of BIKDD and IRE1α inhibitor for treating TNBC.

Next, we evaluated the anti-tumor activity of this combinatory treatment strategy in animal models. To this end, Hs578T cells expressing CMV-BIKDD or control vector were orthotopically transplanted into the mammary fat pad of nude mice, followed by administration of STF-083010 (Fig. 8 D, left panel). While administration of BIKDD or STF-083010 alone resulted in a modest reduction of tumor growth, combined treatment greatly suppressed tumor growth (Fig. 8 D, middle and right panels). To improve the therapeutic feasibility, we adopted a previously established gene therapy protocol via liposome-assisted delivery of VISA-BIKDD (Lang et al., 2011) and combined this gene therapy approach with STF-083010 administration for treating nude mice bearing orthotopic breast tumors derived from Hs578T cells (Fig. 8 E, left panel). With this model, we again observed a significant enhancement of the anti-tumor effect by combined administration of BIKDD and STF-083010 compared to treatment with BIKDD alone (Fig. 8 E, middle and right panels). Importantly, the body weights of mice were not altered by combined treatment in either model (Fig. S5, K and L), implicating the lack of toxicity. These findings indicate that targeting the ASB11-dependent BIK degradation pathway could be exploited to enhance the anti-tumor efficacy of BIKDD-based gene therapy.

Discussion

In this study, we employed an unbiased screening to identify Cul5-ASB11 as a ubiquitin ligase targeting BIK for
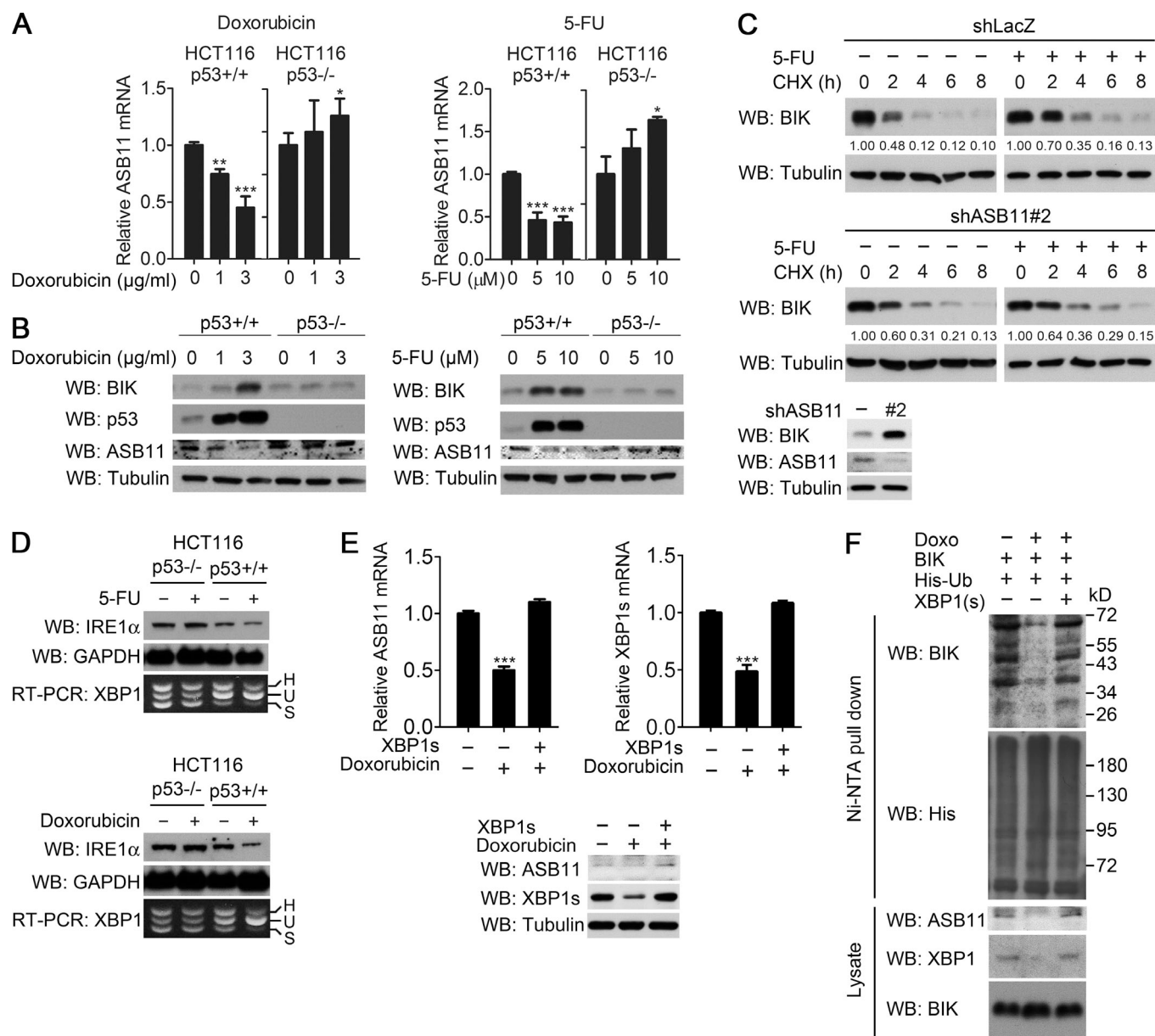
Chen et al.
BIK degradation in controlling stress responses

Journal of Cell Biology 3009
https://doi.org/10.1083/jcb.201901156

Figure 5. DNA damage–induced p53 suppresses XBP1 and ASB11 to stabilize BIK. (A) RT-qPCR analysis of *ASB11* mRNA expression in indicated HCT116 cells treated with the indicated dosages of doxorubicin or 5-FU for 24 h. Data are mean ± SD; *P < 0.05, **P < 0.01, ***P < 0.001 by t test; n = 3. **(B)** Western blot (WB) analysis of BIK and ASB11 expression in the indicated HCT116 cells treated as in A. **(C)** HCT116 p53$^{+/+}$ cells stably expressing control or ASB11 shRNA were treated with 10 μM 5-FU for 24 h and then with cycloheximide (CHX) for the indicated time points. Cells were lysed for Western blot analysis of BIK expression. For a clear comparison, the exposure times of the four BIK blots were adjusted to make the initial points (time 0) with similar intensities. The relative amounts of BIK are indicated by assigning the values from the initial time point as 1. The expression levels of ASB11 and BIK in the stable lines are shown in the bottom panel. **(D)** Western blot analysis of IRE1α expression and RT-PCR analysis of *XBP1* mRNA splicing in the indicated HCT116 cells treated with 3 μg/ml doxorubicin or 10 μM 5-FU for 24 h. The unspliced (U), spliced (S), and hybrid (H) forms of XBP1 are indicated. **(E)** RT-qPCR and Western blot analyses of ASB11 and XBP1s expression in HCT116 cells transfected with XBP1s and/or treated with 3 μg/ml doxorubicin for 24 h. Data are mean ± SD; ***P < 0.001 by t test; n = 3. **(F)** Analysis of BIK ubiquitination in HCT116 cells transfected with the indicated constructs and/or treated with 3 μg/ml doxorubicin for 24 h.

polyubiquitination, thereby promoting its proteasomal degradation. The involvement of a CRL ubiquitin ligase in BIK ubiquitination is consistent with a previous report showing an elevation of BIK protein level by the neddylation inhibitor MLN4924 (Wang et al., 2015). Furthermore, the subcellular localization of ASB11 coincides with BIK. We subsequently show that *ASB11* mRNA is induced under ER stress and repressed

under DNA damage, and the two stress pathways converge on XBP1s, which binds to the *ASB11* promoter through NF-Y to stimulate *ASB11* transcription. In line with these opposite regulations of ASB11, BIK ubiquitination and degradation are enhanced under ER stress and attenuated in response to DNA damage, thereby contributing to cell adaptation and apoptosis, respectively. Our study thus reveals a central role of
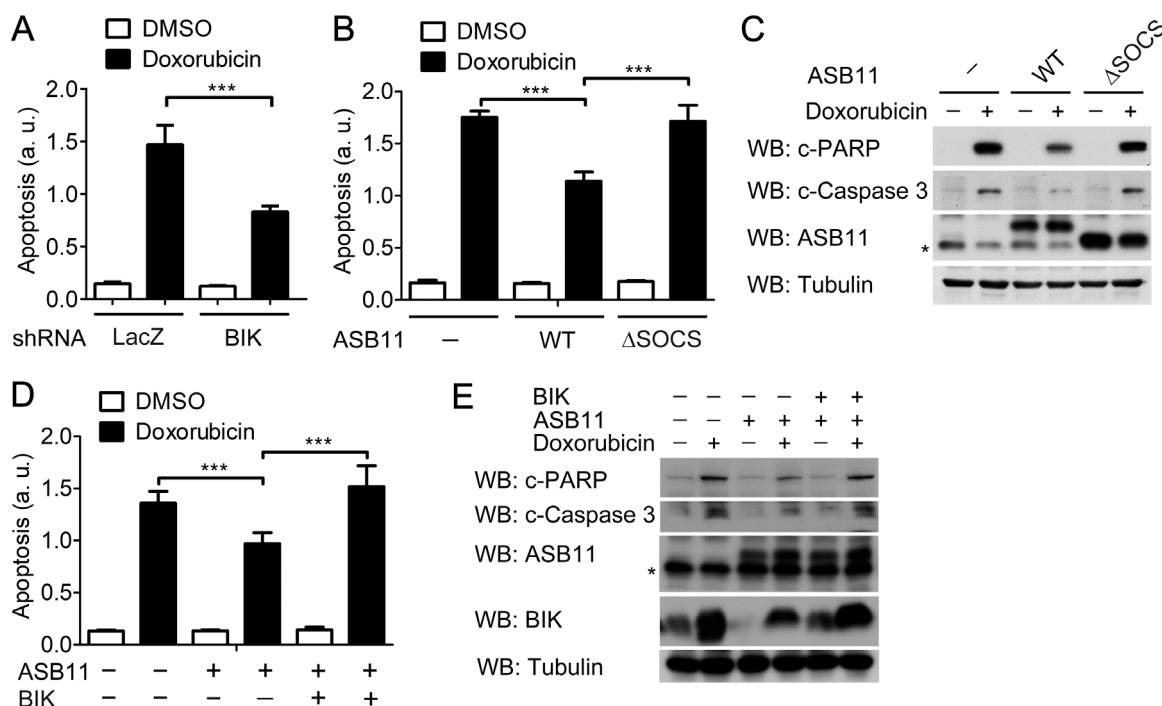
Figure 6. **Regulation of ASB11-mediated BIK ubiquitination influences on cell life/death decision under DNA damage. (A)** ELISA assay for cell apoptosis in HCT116 p53$^{+/+}$ cells stably expressing BIK shRNA. **(B and C)** ELISA assay of cell apoptosis (B) and Western blot (WB) analysis of active caspase 3 and cleaved PARP (C) in HCT116 p53$^{+/+}$ cells stably expressing the indicated ASB11 constructs and treated with 3 μg/ml doxorubicin for 24 h. **(D and E)** ELISA assay of cell apoptosis (D) and Western blot analysis of active caspase 3 and cleaved PARP (E) in HCT116 p53$^{+/+}$ cells transiently transfected with ASB11 and/or BIK and treated with 3 μg/ml doxorubicin for 24 h. Data in A, B, and D are mean ± SD; ***P < 0.001 by one-way ANOVA with Tukey's post hoc test; n = 3. Asterisks in C and E denote a nonspecific band.

ASB11-mediated BIK ubiquitination in determining the life/death cell fate under two different stress conditions.

The finding that BIK degradation can be triggered by the IRE1α–XBP1s axis is exploited for designing an improved anticancer strategy. We show that a combinatory administration of BIKDD and IRE1α inhibitor increases BIKDD stability to lead to a synergistic killing effect on TNBC cells. In theory, the IRE1α inhibitor could also stabilize endogenous BIK via ASB11 downregulation, which may contribute to a small part of the tumor-killing effect of combined treatment. In an orthotopic TNBC model, this combined treatment completely blocks tumor growth, which cannot be achieved by treatment with BIKDD alone. We believe that this combinatory treatment strategy can be applied to other cancer types. Furthermore, with the recent development of IRE1α endonuclease inhibitors (Sanches et al., 2014), more options can be exploited in vivo to obtain a desired therapeutic effect. Of note, since IRE1α acts downstream of p53, the anti-tumor effect of combined treatment is independent of p53 status. Indeed, the beneficial effect of combined treatment is observed in tumor cells expressing mutant p53 (Hs578T and MDA-MB468) or without expressing p53 (MDA-MB157).

In response to ER stress, cells activate UPR to restore ER homeostasis. However, if stress persists or cannot be effectively resolved, UPR signaling becomes pro-apoptotic. It has been shown that the pro-apoptotic UPR up-regulates the BH3-only proteins BIM and PUMA and down-regulates the pro-survival Bcl-2 protein, and these events could act in concert to contribute to cell death (McCullough et al., 2001; Puthalakath et al., 2007; Cazanave et al., 2010). In the adaptive phase of UPR, our discovery for the induction of ASB11-dependent BIK degradation by IRE1α–XBP1 represents the first evidence for the regulation of a Bcl-2 family protein in this period. This mechanism, in conjunction with the decay of death receptor 5 mRNA catalyzed by IRE1α (Lu et al., 2014), would prevent premature apoptotic activation from both intrinsic and extrinsic pathways to allow time for cell adaptation to ER stress.

The precise mechanisms underlying the switch of UPR from cytoprotection to apoptosis have not been completely understood. Previous studies indicated that persistent ER stress deactivates the IRE1α–XBP1 axis, whereas PERK signaling is maintained persistently (Lin et al., 2007; Li et al., 2010). A recent study further revealed that PERK signaling is responsible for this IRE1α deactivation through RPAP2-mediated IRE1α dephosphorylation (Chang et al., 2018). Importantly, the difference in the signaling duration between the IRE1α and PERK axis plays a crucial role in switching cell fate from cytoprotection to apoptosis, as the apoptotic effectors of UPR are mainly induced by the PERK axis (Rodriguez et al., 2011; Chang et al., 2018). Consistent with the regulation of BIK stability by the IRE1α–XBP1 axis, we show that BIK destabilization in response to ER stress similarly adopts a transient mode and occurs only in the adaptive phase of UPR. During prolonged ER stress, BIK is no longer destabilized and can be further activated by release from BiP sequestration through a reduction of BiP translation (López
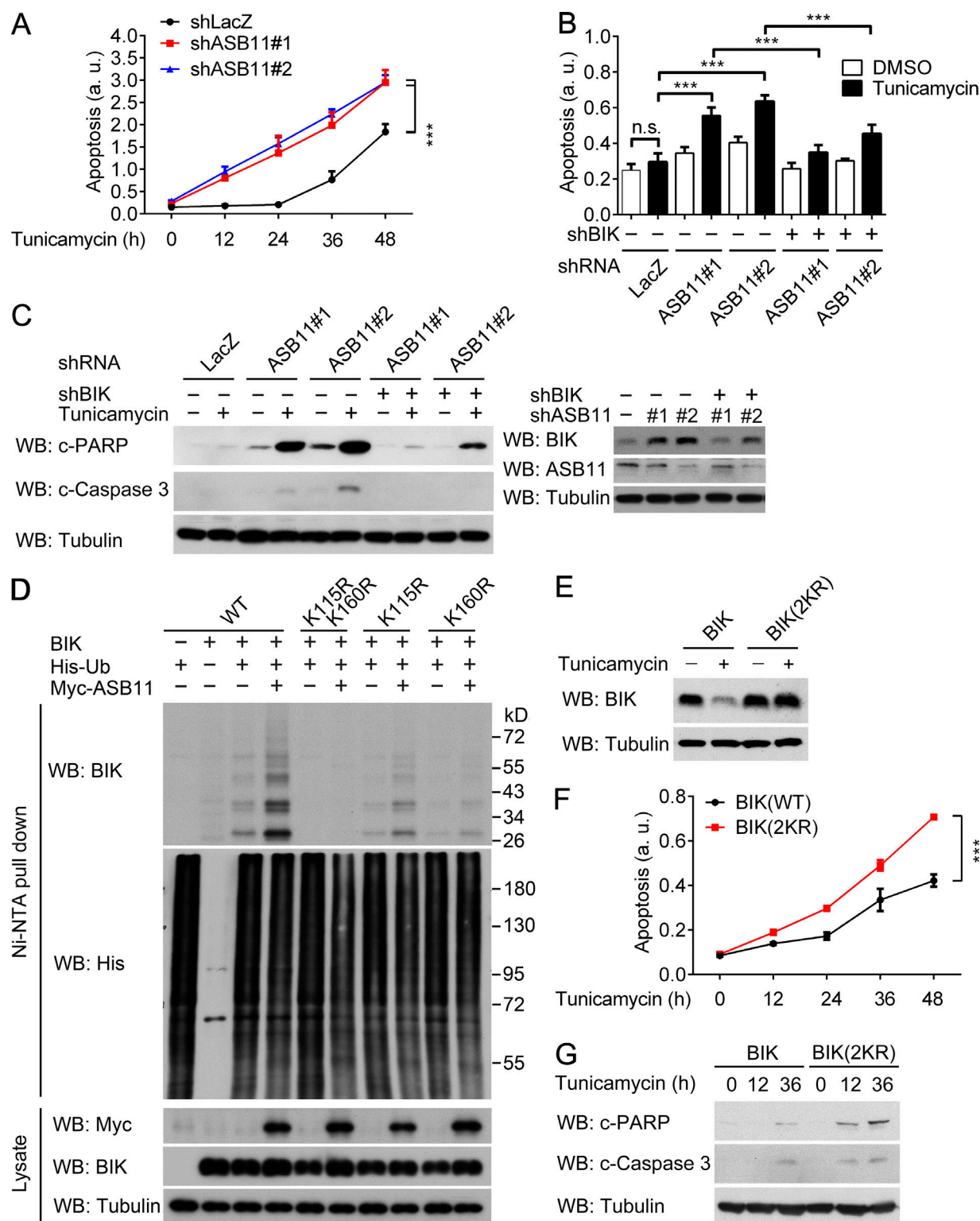
Chen et al.
BIK degradation in controlling stress responses

Journal of Cell Biology
https://doi.org/10.1083/jcb.201901156

3011

Figure 7. **Regulation of ASB11-mediated BIK ubiquitination influences on cell life/death decision under ER stress. (A–C)** ELISA assay for cell apoptosis (A and B) and Western blot (WB) analysis of active caspase 3 and cleaved PARP (C) in 293T cells stably expressing the indicated shRNAs and treated with 10 µg/ml tunicamycin for the indicated time points (A) or for 12 h (B and C). The knockdown efficiencies of various shRNAs are shown in the right panel of C. n.s., not significant. **(D)** Analysis of ubiquitination of wild-type and mutant BIK in 293T cells transfected with the indicated constructs. The ubiquitinated proteins were pulled down under denaturing conditions by Ni-NTA agarose and analyzed by Western blot. **(E)** Western blot analysis of BIK level in BIK knockdown 293T cells transiently transfected with the indicated BIK constructs and treated with 10 µg/ml tunicamycin for 16 h. The equal expression of BIK and BIK(2KR) in untreated cells (by adjusting the amount of plasmid used for transfection) is shown. **(F and G)** ELISA assay of apoptotic cells (F) and Western blot analysis of active caspase 3 and cleaved PARP (G) in 293T cells transfected using the same conditions as in E and treated with 10 µg/ml tunicamycin for the indicated time points. Data in A, B, and F are mean ± SD; ***P < 0.001 by one-way ANOVA with Tukey's post hoc test; n = 3. n.s., not significant.
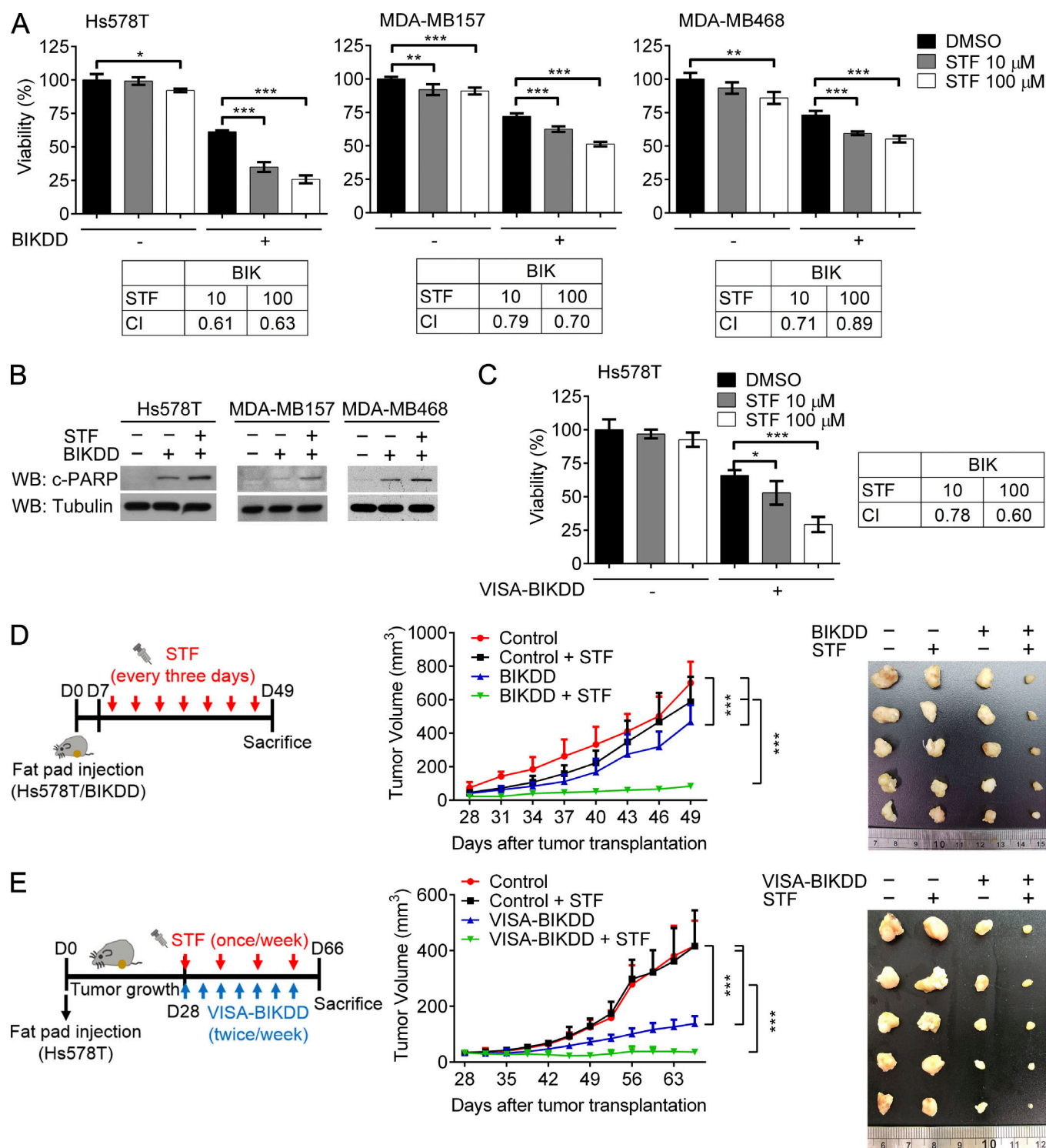
Figure 8. **IRE1α inhibitor enhances the tumor-killing effect of BIKDD. (A and C)** MTT assay for the viability of the indicated TNBC cells transfected with 0.5 µg CMV-BIKDD (A) or VISA-BIKDD (C) and treated with 10 or 100 µM STF-083010 for 48 h. Data are mean ± SD; *P < 0.05, **P < 0.01, ***P < 0.001 by one-way ANOVA with Tukey's post hoc test; n = 3. CI values are indicated. **(B)** Western blot (WB) analysis of cleaved PARP in the indicated TNBC cells transfected with CMV-BIKDD and treated with 100 µM STF-083010 for 36 h. **(D)** Mice orthotopically implanted with Hs578T cells carrying BIKDD or control vector and treated with STF-083010 or DMSO (left panel). Tumor volumes were measured at the indicated days and plotted (middle panel). Data are mean ± SD; ***P < 0.001 by two-way ANOVA with Tukey's post hoc test; n = 5. Tumors were surgically removed at day 49, and their sizes are shown on the right. **(E)** Mice orthotopically implanted with Hs578T cells and treated with VISA-BIKDD liposome nanoparticle together with STF-083010 or DMSO starting at day 28 after tumor cell implantation (left panel). Tumor volumes were measured at the indicated days and plotted (middle panel). Data are mean ± SD; ***P < 0.001 by two-way ANOVA with Tukey's post hoc test; n = 5. Tumors were surgically removed at day 66, and their sizes are shown on the right.

et al., 2017). We believe that this biphasic regulation of BIK a-bundance/activity would account for an additional mechanism by which cells transit from the adaptive to the apoptotic phase of UPR.

The stimulation of BIK proteasomal degradation by ER stress and the requirement of p97 for this degradation resemble the ERAD process. However, BIK degradation is fundamentally different from ERAD in at least two aspects. First, BIK degradation is mediated by Cul5-ASB11, rather than ERAD ubiquitin ligases (Ruggiano et al., 2014). Second, unlike canonical ERAD substrates whose degradation is mainly restricted to the misfolded/damaged form, the native/functional BIK is subjected to degradation, as blockage of this degradation by ASB11 depletion enhances cell apoptosis. Thus, BIK degradation under ER stress plays a regulatory, rather than a quality-control, role. Importantly, the induction of ER-residing ASB11 by ER stress raises the possibility that Cul5-ASB11 governs a novel degradation program associated with ER stress. It would be important to systematically identify Cul5-ASB11 substrates for a more complete understanding of the contribution of this E3 ligase to cell fitness under ER stress.

In contrast to ER stress, DNA damage leads to ASB11 down-regulation and BIK stabilization through a p53-dependent mechanism. However, in cells without expressing p53 (HCT116) or expressing a mutant p53 (H1299), DNA damage leads to a slight elevation of ASB11 level. Since there is no evidence of an activation of an IRE1α pathway by DNA damage, it would require further study to dissect the underlying mechanism. Notably, DNA damage also increases BIK mRNA (Hur et al., 2006), as BIK is a direct transcriptional target of p53 (Mathai et al., 2002). Thus, our finding for the enhancement of BIK protein stability represents an additional layer of the BIK regulatory mechanism in response to DNA damage. It is likely that through both transcriptional and posttranslational mechanisms, BIK level can reach a threshold for an effective induction of apoptosis. Intriguingly, the DNA damage–p53 axis also acts through the IRE1α–XBP1 pathway to regulate ASB11. Consistent with a previous report (Namba et al., 2015), we show that p53 reduces IRE1α abundance even in the absence of ER stress inducers, thereby diminishing the basal level of XBP1 mRNA splicing. This finding not only provides a mechanistic insight into the ASB11 down-regulation and BIK stabilization induced by DNA damage, but also uncovers an intriguing crosstalk between different cellular stress pathways.

Our study indicates that XBP1s is recruited to the ASB11 promoter via the general transcription factor NF-Y. The interplay between NF-Y and XBP1s in the transcriptional responses to ER stress has long been known. One type of the authentic XBP1s binding motif, called ERSE, is composed of an NF-Y binding site and an XBP1 binding site, which are separated by a short stretch of nucleotides (Yamamoto et al., 2004). While XBP1s binding to ERSE is induced by ER stress, NF-Y binding is constitutive (Donati et al., 2006). However, different from the previously identified cooperative action of XBP1s and NF-Y on ERSE, XBP1s is recruited to the ASB11 promoter via its physical interaction with NF-Y, rather than through its direct binding to DNA. This new cooperative mode is likely applied to other XBP1-target promoters that contain only the NF-Y binding motif (Acosta-Alvear et al., 2007).

In conclusion, our study identifies Cul5-ASB11 as a ubiquitin ligase for BIK. ASB11 is positively and negatively regulated by ER stress and DNA damage, respectively, which results in opposite regulations of BIK protein abundance and cell life/death fate under the two cellular stresses. Targeting the ASB11-dependent BIK degradation pathway can be exploited in combination with the active BIK gene therapy for an effective anti-cancer strategy.

Materials and methods

Antibodies and reagents
The ASB11 antiserum was generated and affinity purified by LTK BioLaboratories Inc. using the peptide TDYGANLKRRNAQGKSAL (corresponding to amino acids 248–265 of ASB11) as an antigen. Other antibodies used in this study are described in Table S1. Cycloheximide, doxorubicin, 5-FU, 4μ8C, STF-083010, tunicamycin, and thapsigargin were purchased from Sigma-Aldrich. MG132 was obtained from Calbiochem, whereas CB-5083 was from Cayman Chemical.

Cell culture and transfection
293T, 293FT, H1299, Hs578T, MDA-MB157, and MDA-MB468 cells were maintained in DMEM supplemented with 10% FCS, 100 U/ml penicillin, and 100 μg/ml streptomycin. HCT116 cells were cultured in RPMI-1640 with 10% FCS, 100 U/ml penicillin, and 100 μg/ml streptomycin. Transfection was performed using the calcium phosphate method or the Lipofectamine 3000 reagent.

Plasmids
All Cullin DN mutant constructs were generated by site-directed mutagenesis from wild-type constructs obtained from Hsueh-Chi Sherry Yen (Academia Sinica, Nankang, Taipei, Taiwan). BIK cDNA was subcloned to 3XFlag–pCMV7.1.2 vector or pRK5, and BIK mutants were generated by site-directed mutagenesis. XBP1s was PCR amplified from cDNAs derived from tunicamycin-treated HeLa cells and cloned to pRK5. Among the cDNAs of Cul5 substrate adaptors, SSB2 was from Soichi Miwa (Hokkaido University, Sapporo, Hokkaido, Japan); RAB40A and RAB40C were from John H. Brumell (University of Toronto, Toronto, Ontario, Canada); RAB40B was from Jorge E. Galán (Yale University, New Haven, CT); WSB2 was from Yue Xiong (University of North Carolina at Chapel Hill, Chapel Hill, NC); CIS was from Lu-Hai Wang (National Health Research Institutes, Zhunan, Miaoli, Taiwan); SSB1, SSB3, and SSB4 were from Guan Wu (University of Rochester Medical Center, Rochester, NY); ASB1, ASB6, ASB7, and ASB12 were from Yasuhiko Masuho (Tokyo University of Science, Noda, Chiba, Japan); and ASB3, WSB1, PCMTD2, and Muf1 were from Joan Conaway (The University of Kansas School of Medicine, Kansas City, KS). Other substrate adaptors were amplified from mRNA derived from 293T cells. All substrate adaptors were cloned to pRK5-Flag. The primers used for amplifying these cDNAs are listed in Table S2. HA-ElonginB and T7-ElonginC were provided by Dong Xie (Shanghaitech University, Pudong, Shanghai, China), and ROC2

Chen et al.
BIK degradation in controlling stress responses

Journal of Cell Biology   3014
https://doi.org/10.1083/jcb.201901156

cDNA was provided by Yue Xiong (University of North Carolina at Chapel Hill, Chapel Hill, NC). His-ubiquitin was described previously (Yuan et al., 2011). p53 cDNA was obtained from Sheau-Yann Shieh (Academia Sinica, Nankang, Taipei, Taiwan) and subcloned to pRK5. CMV-BIKDD and VISA-BIKDD were described previously (Lang et al., 2011). pGL4-ERSE1-luc2P-Hygro was obtained from Addgene.

RNA interference

Lentivirus-based constructs were obtained from the National RNAi Core Facility, Taiwan. The shRNA target sequences are listed in Table S3. To generate recombinant lentivirus carrying shRNAs, 293FT cells were cotransfected with the packaging plasmid pCMVDR8.91, envelope plasmid pMD.G, and shRNA-expressing construct. For infection, the viral stock was supplemented with 8 µg/ml polybrene, and infected cells were selected by appropriated agents.

Immunoprecipitation and Western blot

Cell extraction was performed with radioimmunoprecipitation assay lysis buffer containing 50 mM Tris (pH 8.0), 0.15 M NaCl, 1% NP-40, 1% sodium deoxycholate, 0.1% SDS, 1 mM PMSF, 1 µg/ml aprotinin, and 1 µg/ml leupeptin. Western blot was performed with the standard protocol. For an efficient detection of BIK by Western blot, tricine SDS-PAGE was used. Western blot analyses of other proteins were performed with glycine SDS-PAGE. Immunoprecipitation was performed and analyzed as previously described (Liu et al., 2016). Briefly, cell lysates were incubated with primary antibody overnight. PureProteome Protein A/G Magnetic Beads (LSKMAGA/G10; EMD Millipore) were then added into cell lysates and incubated for 1.5 h. The beads were washed with radioimmunoprecipitation assay lysis buffer, and the bound proteins were analyzed by Western blot.

Ubiquitination assays

For in vitro ubiquitination assay, ASB11-based Cul5 E3 ligase complex and 3xFlag-BIK were separately purified using anti-Flag M2 affinity agarose gel (Sigma-Aldrich) from lysates of 293T cells transfected with 3xFlag-BIK, or cotransfected with Flag-ASB11, Myc-Cul5, V5-ROC2, T7-ElonginC, and HA-ElonginB. 3xFlag-BIK was eluted from the beads with elution buffer containing 150 mg/ml 3X FLAG Peptide (Sigma-Aldrich), 50 mM Tris-HCl (pH 7.4), and 150 mM NaCl at room temperature for 1 h. The E3 ligase complex bound on beads was incubated at 37°C for 2 h in a 20-µl ubiquitination reaction mixture containing 40 ng yeast E1, 500 ng E2 (UbcH5a), 300 ng 3xFlag-BIK, and other components as described previously (Yuan et al., 2011). The E1, E2, His-ubiquitin, and other related reagents used in this assay were purchased from R&D Systems.

For the in vivo ubiquitination assay, cells were transfected with various constructs and His-ubiquitin and treated with 1 µM MG132 for 16 h. Cells were lysed under denaturing conditions by buffer A (6 M guanidine-HCl, 0.1 M Na_2HPO_4/NaH_2PO_4, pH 8.0, and 10 mM imidazole), and lysates were incubated with nickel–nitrilotriacetic acid (Ni-NTA) Sepharose, a nickel-charged affinity resin that can be used to purify recombinant proteins containing a polyhistidine (6xHis) sequence, at 4°C for 2 h. The beads were washed once with buffer A, twice with buffer A/TI (1:3 vol buffer A/buffer TI [25 mM Tris-HCl, pH 6.8, and 20 mM imidazole]), and three times with buffer TI and then were incubated in the sample buffer at 95°C for 5 min. In all experiments, equal expression of His-ubiquitin was verified by Western blot analysis.

MS analysis of the ubiquitination site

For identification of the ubiquitination site on BIK, Flag-BIK was purified from 293T cells transfected with His-ubiquitin, Myc-ASB11, and Flag-BIK using anti-Flag M2 affinity agarose gel (Sigma-Aldrich) and then resolved by SDS-PAGE. Specific ubiquitinated bands were cut out from the gel and were subjected to mass spectrometric peptide sequencing. Briefly, gel slices were destained with 50% acetonitrile (ACN)/25 mM ammonium bicarbonate, reduced by 5 mM dithioerythritol, and alkylated by adding 10 mM iodoacetamide. Gel slices were then washed four times with 50% ACN/25 mM ammonium bicarbonate and dried by soaking in 100% ACN. After evaporating ACN, proteins were digested with trypsin (Promega; v5117) and Glu-C (Promega; v1651) for 18 h. Next, peptides were extracted by adding 50% ACN/5% trifluoroacetic acid. The supernatant was desalted by Zip-Tip and lyophilized for MS analysis.

NanoLC-nanoESi-MS/MS analysis was performed on a Thermo UltiMate 3000 RSLCnano system connected to a Thermo Orbitrap Fusion mass spectrometer (Thermo Fisher Scientific) equipped with a nanospray interface (New Objective). Peptide mixtures were loaded onto a 75-µm inner diameter, 25-cm-long PepMap C18 column (Thermo Fisher Scientific) packed with 2-µm particles with a pore size of 100 Å and were separated using a segmented gradient in 120 min from 5% to 35% solvent B (0.1% formic acid in ACN) at a flow rate of 300 nl/min. Solvent A was 0.1% formic acid in water. The mass spectrometer was operated in the data-dependent mode. Briefly, survey scans of peptide precursors from 350 to 1,600 m/z were performed at 120-K resolution with a 2×10^5 ion count target. Tandem MS was performed by isolation window at 1.6 D with the quadrupole, higher-energy collisional dissociation fragmentation with a normalized collision energy of 30, and MS^2 scan analysis at 30-K resolution in the orbitrap. The MS^2 ion count target was set to 5×10^4, and the max injection time was 54 ms. Only those precursors with a charge state of 2–6 were sampled for MS^2. The instrument was run in top-speed mode with 3-s cycles, and the dynamic exclusion duration was set to 15 s with a 10-ppm tolerance around the selected precursor and its isotopes. Monoisotopic precursor selection was turned on. The raw data obtained from liquid chromatography with tandem MS acquisition was processed using Proteome Discoverer (version 2.3; Thermo Fisher Scientific), searching files using Mascot search engine (v.2.6.0; Matrix Science) against the customized Swiss-Prot Homo sapiens database (20,422 sequences) and Flag-tagged BIK. The search criteria used were trypsin and Glu-C digestion, allowing up to two missed cleavages, mass accuracy of 10 ppm for the parent ion, and 0.02 D for the fragment ions. Fixed modifications were set as carbamidomethyl (cysteine), and variable modifications were set as oxidation (methionine), GlyGly (lysine), and LeuArgGlyGly (lysine). A decoy database

Chen et al.
BIK degradation in controlling stress responses

Journal of Cell Biology   3015
https://doi.org/10.1083/jcb.201901156

search was performed. Identified peptides were filtered with a 1% false discovery rate and peptide-spectrum match. Ubiquitination sites and peptide sequence assignments contained in MASCOT search results were validated by manual confirmation from raw MS/MS data.

Apoptosis assay

Apoptosis was analyzed as previously described (Liu et al., 2016). Briefly, cells were seeded at a density of 10^6 cells in a 6-cm dish overnight. The cells were then incubated with doxorubicin or tunicamycin for various time points. Cells were harvested with 250 µl lysis buffer (Cell Death ELISA Kit; Roche). The lysate was centrifuged at 200 g for 5 min, and 20 µl supernatant was incubated with immunoreagent containing 4 µl anti–histone-biotin, 4 µl anti–DNA-POD, and 72 µl incubation buffer (Cell Death ELISA Kit) at room temperature for 2 h in the streptavidin-coated well of the microplate. The reaction mixture was removed, and the well was washed three times with 250 µl of incubation buffer. Next, the well was incubated with 100 µl ABTS substrate solution (Cell Death ELISA Kit) at room temperature for 5 min, followed by absorbance measurement at 405 nm.

Quantitative real-time PCR (RT-qPCR)

Total mRNA was extracted from cells using TRIZOL reagent (Invitrogen), and equal amounts of RNA were reverse transcribed to cDNA using the iScript cDNA Synthesis Kit (Bio-Rad). RT-qPCR was performed using the Power SYBR Green PCR Master kit (Applied Biosystems). Amplification was performed on an ABI 7500 Fast Real-Time PCR system, and GAPDH was used as an internal control. The PCR primer sequences are described in Table S2.

Luciferase reporter assay

Cells were cotransfected with pGL3-based reporter construct and pTK-renilla plasmid, together with other constructs, for 24 h. Luciferase reporter assay was performed by the dual-luciferase reporter assay system (Promega) according to the manufacturer's instructions. The relative promoter activity was expressed as the fold change in firefly luciferase activity after normalization to the renilla luciferase activity.

ChIP assay

ChIP assay was performed as previously described (Wu et al., 2014). Briefly, 293T cells were seeded at a density of 10^7 cells in a 10-cm dish overnight. The cells were treated with tunicamycin for 4 h and then fixed with 1% formaldehyde at room temperature for 10 min. The reaction was stopped with 125 mM glycine for 5 min. Cells were lysed with ChIP lysis buffer containing 50 mM Tris (pH 7.5), 150 mM NaCl, 5 mM EDTA, 0.5% NP-40, 1% Triton X-100, 0.005% SDS, 1 mM PMSF, 1 µg/ml aprotinin, and 1 µg/ml leupeptin. The lysates were sonicated for shearing DNA and then incubated with XBP1 antibody or ChIP-grade rabbit IgG (as a control) at 4°C for 16 h. The immunocomplexes were purified using protein A magnetic beads and sequentially washed five times with wash buffer I (1 M Hepes, pH 7.5, 0.5 M EDTA, 10% NP-40, 6 M LiCl, 10% sodium deoxycholate, 1 mM PMSF, 1 µg/ml aprotinin, and 1 µg/ml leupeptin) and one time with wash buffer II (10 mM Tris, pH 8.0, 1 mM EDTA, and 50 mM NaCl). The immunoprecipitated DNA was isolated from the beads by incubation with 200 µl elution buffer containing 10 mM Tris (pH 8.0), 1 mM EDTA, 0.5% SDS, and 250 mM NaCl at 65°C for 20 min. The eluted solution was then incubated with 5 µl RNase (EN0531; Thermo Fisher Scientific) at 37°C for 5 min. DNA from the eluted solution was purified using a DNA mini kit (51306; QIAGEN). Enrichment of the promoter binding level was analyzed by quantitative PCR (qPCR). The qPCR primers for ChIP assay are listed in Table S2.

MTT assay

MDA-MB157 and MDA-MB468 cells were seeded at a density of 5×10^3 cells, and Hs578T cells were seeded at a density of 2×10^3 cells in 96-well plates. Cells were transfected with BIKDD. The next day, cells were treated with IRE1α inhibitor or DMSO for 48 h and then with 0.4 mg/ml methyl thiazolyl diphenyl tetrazolium bromide (MTT; Sigma-Aldrich) for 2 h. Cells were dissolved in DMSO, followed by absorbance measurement at 590 nm. The combination index (CI) was calculated using the equation $CI = C_A/IC50_A + C_B/IC50_B$. C_A and C_B represent the concentrations of the two agents for combined treatment. $IC50_A$ and $IC50_B$ are the IC50 values for each single treatment, which were determined by treating cells with increasing dosages of each agent followed by MTT assay. $CI < 1$ indicates a synergistic effect, $CI > 1$ corresponds to an antagonistic effect, and $CI = 1$ represents an additive effect.

Animal experiments

All mice were maintained according to the guidelines of animal ethical regulations, and all animal studies were approved by the Experimental Animal Committee, Academia Sinica. 5-wk-old female BALB/cAnN.Cg-Foxnlnu/CrlNarl nude mice (National Laboratory Animal Center) were inoculated in the mammary fat pad with 2×10^6 Hs578T cells transiently expressing BIKDD or control vector. 7 d later, DMSO or STF-083010 (40 mg/kg) was intraperitoneally administrated every 3 d. For BIKDD gene therapy protocol, 5-wk-old female BALB/cAnN.Cg-Foxnlnu/CrlNarl nude mice (National Laboratory Animal Center) were inoculated in the mammary fat pad with 2×10^6 Hs578T cells. 28 d later, DMSO or STF-083010 (40 mg/kg) was intraperitoneally administrated every 3–4 d. Control vector or VISA-BIKDD (0.75 mg/kg) was first incubated with the in vivo jetPEI delivery reagent (PEI; Polyplus Transfection) for 15 min, and then the complex was intratumorally injected every 7 d starting at day 28. For both models, tumors were measured every 3 or 4 d, and their volumes were calculated using the equation $mm^3 = \pi/6 \times [length (mm)] \times [width (mm)]^2$.

Statistical analysis

All graphs show means with error bars representing SD of a minimum of three biological replicates. Statistical analysis was performed using two-tailed Student's t tests for comparisons between two groups and one-way or two-way ANOVA with Tukey's post hoc test for multigroup comparisons. All statistical analyses were conducted at a significance level of $P < 0.05$.

Online supplemental material

Fig. S1 shows that ASB11 targets BIK to the Cul5 complex for ubiquitination. Fig. S2 shows that ASB11 and XBP1 mediate ER stress–induced BIK degradation. Fig. S3 shows that DNA damage acts through p53 to down-regulate ASB11. Fig. S4 shows the characterizations of BIK ubiquitination site and BIK(2KR) mutant. Fig. S5 shows that BIKDD is a target of ASB11 and that its stability and tumor-killing effect are enhanced by IRE1α inhibitor. Table S1 provides information for antibodies used in this study. Table S2 contains the primers for PCR, qPCR, and cloning. Table S3 provides the targeting sequences for shRNAs.

References

Acosta-Alvear, D., Y. Zhou, A. Blais, M. Tsikitis, N.H. Lents, C. Arias, C.J. Lennon, Y. Kluger, and B.D. Dynlacht. 2007. XBP1 controls diverse cell type- and condition-specific transcriptional regulatory networks. *Mol. Cell.* 27:53–66. https://doi.org/10.1016/j.molcel.2007.06.011

Andresen, C.A., S. Smedegaard, K.B. Sylvestersen, C. Svensson, D. Iglesias-Gato, G. Cazzamali, T.K. Nielsen, M.L. Nielsen, and A. Flores-Morales. 2014. Protein interaction screening for the ankyrin repeats and suppressor of cytokine signaling (SOCS) box (ASB) family identify Asb11 as a novel endoplasmic reticulum resident ubiquitin ligase. *J. Biol. Chem.* 289:2043–2054. https://doi.org/10.1074/jbc.M113.534602

Avci, D., and M.K. Lemberg. 2015. Clipping or Extracting: Two Ways to Membrane Protein Degradation. *Trends Cell Biol.* 25:611–622. https://doi.org/10.1016/j.tcb.2015.07.003

Boyd, J.M., G.J. Gallo, B. Elangovan, A.B. Houghton, S. Malstrom, B.J. Avery, R.G. Ebb, T. Subramanian, T. Chittenden, R.J. Lutz, et al. 1995. Bik, a novel death-inducing protein shares a distinct sequence motif with Bcl-2 family proteins and interacts with viral and cellular survival-promoting proteins. *Oncogene.* 11:1921–1928.

Cazanave, S.C., N.A. Elmi, Y. Akazawa, S.F. Bronk, J.L. Mott, and G.J. Gores. 2010. CHOP and AP-1 cooperatively mediate PUMA expression during lipoapoptosis. *Am. J. Physiol. Gastrointest. Liver Physiol.* 299:G236–G243. https://doi.org/10.1152/ajpgi.00091.2010

Chang, T.K., D.A. Lawrence, M. Lu, J. Tan, J.M. Harnoss, S.A. Marsters, P. Liu, W. Sandoval, S.E. Martin, and A. Ashkenazi. 2018. Coordination between Two Branches of the Unfolded Protein Response Determines Apoptotic Cell Fate. *Mol. Cell.* 71:629–636.e5. https://doi.org/10.1016/j.molcel.2018.06.038

Chen, L., S.N. Willis, A. Wei, B.J. Smith, J.I. Fletcher, M.G. Hinds, P.M. Colman, C.L. Day, J.M. Adams, and D.C. Huang. 2005. Differential targeting of prosurvival Bcl-2 proteins by their BH3-only ligands allows complementary apoptotic function. *Mol. Cell.* 17:393–403. https://doi.org/10.1016/j.molcel.2004.12.030

Chen, X., D. Iliopoulos, Q. Zhang, Q. Tang, M.B. Greenblatt, M. Hatziapostolou, E. Lim, W.L. Tam, M. Ni, Y. Chen, et al. 2014. XBP1 promotes triple-negative breast cancer by controlling the HIF1α pathway. *Nature.* 508:103–107. https://doi.org/10.1038/nature13119

Dehan, E., F. Bassermann, D. Guardavaccaro, G. Vasiliver-Shamis, M. Cohen, K.N. Lowes, M. Dustin, D.C. Huang, J. Taunton, and M. Pagano. 2009. betaTrCP- and Rsk1/2-mediated degradation of BimEL inhibits apoptosis. *Mol. Cell.* 33:109–116. https://doi.org/10.1016/j.molcel.2008.12.020

del Peso, L., M. González-García, C. Page, R. Herrera, and G. Nuñez. 1997. Interleukin-3-induced phosphorylation of BAD through the protein kinase Akt. *Science.* 278:687–689. https://doi.org/10.1126/science.278.5338.687

Donati, G., C. Imbriano, and R. Mantovani. 2006. Dynamic recruitment of transcription factors and epigenetic changes on the ER stress response gene promoters. *Nucleic Acids Res.* 34:3116–3127. https://doi.org/10.1093/nar/gkl304

Ewings, K.E., K. Hadfield-Moorhouse, C.M. Wiggins, J.A. Wickenden, K. Balmanno, R. Gilley, K. Degenhardt, E. White, and S.J. Cook. 2007. ERK1/2-dependent phosphorylation of BimEL promotes its rapid dissociation from Mcl-1 and Bcl-xL. *EMBO J.* 26:2856–2867. https://doi.org/10.1038/sj.emboj.7601723

Fischer, M., L. Steiner, and K. Engeland. 2014. The transcription factor p53: not a repressor, solely an activator. *Cell Cycle.* 13:3037–3058. https://doi.org/10.4161/15384101.2014.949083

Germain, M., J.P. Mathai, H.M. McBride, and G.C. Shore. 2005. Endoplasmic reticulum BIK initiates DRP1-regulated remodelling of mitochondrial cristae during apoptosis. *EMBO J.* 24:1546–1556. https://doi.org/10.1038/sj.emboj.7600592

Hetz, C., F. Martinon, D. Rodriguez, and L.H. Glimcher. 2011. The unfolded protein response: integrating stress signals through the stress sensor IRE1α. *Physiol. Rev.* 91:1219–1243. https://doi.org/10.1152/physrev.00001.2011

Hur, J., D.W. Bell, K.L. Dean, K.R. Coser, P.C. Hilario, R.A. Okimoto, E.M. Tobey, S.L. Smith, K.J. Isselbacher, and T. Shioda. 2006. Regulation of expression of BIK proapoptotic protein in human breast cancer cells: p53-dependent induction of BIK mRNA by fulvestrant and proteasomal degradation of BIK protein. *Cancer Res.* 66:10153–10161. https://doi.org/10.1158/0008-5472.CAN-05-3696

Kuwana, T., L. Bouchier-Hayes, J.E. Chipuk, C. Bonzon, B.A. Sullivan, D.R. Green, and D.D. Newmeyer. 2005. BH3 domains of BH3-only proteins differentially regulate Bax-mediated mitochondrial membrane permeabilization both directly and indirectly. *Mol. Cell.* 17:525–535. https://doi.org/10.1016/j.molcel.2005.02.003

Lang, J.Y., J.L. Hsu, F. Meric-Bernstam, C.J. Chang, Q. Wang, Y. Bao, H. Yamaguchi, X. Xie, W.A. Woodward, D. Yu, et al. 2011. BikDD eliminates breast cancer initiating cells and synergizes with lapatinib for breast cancer treatment. *Cancer Cell.* 20:341–356. https://doi.org/10.1016/j.ccr.2011.07.017

Letai, A., M.C. Bassik, L.D. Walensky, M.D. Sorcinelli, S. Weiler, and S.J. Korsmeyer. 2002. Distinct BH3 domains either sensitize or activate mitochondrial apoptosis, serving as prototype cancer therapeutics. *Cancer Cell.* 2:183–192. https://doi.org/10.1016/S1535-6108(02)00127-7

Li, C., R. Li, J.R. Grandis, and D.E. Johnson. 2008. Bortezomib induces apoptosis via Bim and Bik up-regulation and synergizes with cisplatin in the killing of head and neck squamous cell carcinoma cells. *Mol. Cancer Ther.* 7:1647–1655. https://doi.org/10.1158/1535-7163.MCT-07-2444

Li, H., A.V. Korennykh, S.L. Behrman, and P. Walter. 2010. Mammalian endoplasmic reticulum stress sensor IRE1 signals by dynamic clustering. *Proc. Natl. Acad. Sci. USA.* 107:16113–16118. https://doi.org/10.1073/pnas.1010580107

Li, L.Y., H.Y. Dai, F.L. Yeh, S.F. Kan, J. Lang, J.L. Hsu, L.B. Jeng, Y.H. Chen, Y.P. Sher, W.C. Lin, and M.C. Hung. 2011. Targeted hepatocellular carcinoma

proapoptotic BikDD gene therapy. *Oncogene.* 30:1773–1783. https://doi .org/10.1038/onc.2010.558

Li, Y.M., Y. Wen, B.P. Zhou, H.P. Kuo, Q. Ding, and M.C. Hung. 2003. Enhancement of Bik antitumor effect by Bik mutants. *Cancer Res.* 63: 7630–7633.

Lin, J.H., H. Li, D. Yasumura, H.R. Cohen, C. Zhang, B. Panning, K.M. Shokat, M.M. Lavail, and P. Walter. 2007. IRE1 signaling affects cell fate during the unfolded protein response. *Science.* 318:944–949. https://doi.org/10 .1126/science.1146361

Liu, C.C., Y.C. Lin, Y.H. Chen, C.M. Chen, L.Y. Pang, H.A. Chen, P.R. Wu, M.Y. Lin, S.T. Jiang, T.F. Tsai, and R.H. Chen. 2016. Cul3-KLHL20 Ubiquitin Ligase Governs the Turnover of ULK1 and VPS34 Complexes to Control Autophagy Termination. *Mol. Cell.* 61:84–97. https://doi.org/10.1016/j .molcel.2015.11.001

López, I., A.S. Tournillon, R. Prado Martins, K. Karakostis, L. Malbert-Colas, K. Nylander, and R. Fåhraeus. 2017. p53-mediated suppression of BiP triggers BIK-induced apoptosis during prolonged endoplasmic reticulum stress. *Cell Death Differ.* 24:1717–1729. https://doi.org/10.1038/cdd .2017.96

Lu, M., D.A. Lawrence, S. Marsters, D. Acosta-Alvear, P. Kimmig, A.S. Mendez, A.W. Paton, J.C. Paton, P. Walter, and A. Ashkenazi. 2014. Opposing unfolded-protein-response signals converge on death receptor 5 to control apoptosis. *Science.* 345:98–101. https://doi.org/10.1126/ science.1254312

Lydeard, J.R., B.A. Schulman, and J.W. Harper. 2013. Building and remodelling Cullin-RING E3 ubiquitin ligases. *EMBO Rep.* 14:1050–1061. https:// doi.org/10.1038/embor.2013.173

Mathai, J.P., M. Germain, R.C. Marcellus, and G.C. Shore. 2002. Induction and endoplasmic reticulum location of BIK/NBK in response to apoptotic signaling by E1A and p53. *Oncogene.* 21:2534–2544. https://doi.org/10 .1038/sj.onc.1205340

Mathai, J.P., M. Germain, and G.C. Shore. 2005. BH3-only BIK regulates BAX,BAK-dependent release of Ca2+ from endoplasmic reticulum stores and mitochondrial apoptosis during stress-induced cell death. *J. Biol. Chem.* 280:23829–23836. https://doi.org/10.1074/jbc .M500800200

Maurel, M., E.P. McGrath, K. Mnich, S. Healy, E. Chevet, and A. Samali. 2015. Controlling the unfolded protein response-mediated life and death decisions in cancer. *Semin. Cancer Biol.* 33:57–66. https://doi.org/10.1016/j .semcancer.2015.03.003

McCullough, K.D., J.L. Martindale, L.O. Klotz, T.Y. Aw, and N.J. Holbrook. 2001. Gadd153 sensitizes cells to endoplasmic reticulum stress by downregulating Bcl2 and perturbing the cellular redox state. *Mol. Cell. Biol.* 21: 1249–1259. https://doi.org/10.1128/MCB.21.4.1249-1259.2001

Mebratu, Y.A., I. Leyva-Baca, M.G. Wathelet, N. Lacey, H.S. Chand, A.M.K. Choi, and Y. Tesfaigzi. 2017. Bik reduces hyperplastic cells by increasing Bak and activating DAPk1 to juxtapose ER and mitochondria. *Nat. Commun.* 8. https://doi.org/10.1038/s41467-017-00975-w

Meyer, H., and C.C. Weihl. 2014. The VCP/p97 system at a glance: connecting cellular function to disease pathogenesis. *J. Cell Sci.* 127:3877–3883. https://doi.org/10.1242/jcs.093831

Nakano, K., and K.H. Vousden. 2001. PUMA, a novel proapoptotic gene, is induced by p53. *Mol. Cell.* 7:683–694. https://doi.org/10.1016/S1097 -2765(01)00214-3

Namba, T., K. Chu, R. Kodama, S. Byun, K.W. Yoon, M. Hiraki, A. Mandinova, and S.W. Lee. 2015. Loss of p53 enhances the function of the endoplasmic reticulum through activation of the IRE1α/XBP1 pathway. *Oncotarget.* 6:19990–20001. https://doi.org/10.18632/oncotarget.4598

Oda, E., R. Ohki, H. Murasawa, J. Nemoto, T. Shibue, T. Yamashita, T. Tokino, T. Taniguchi, and N. Tanaka. 2000. Noxa, a BH3-only member of the Bcl-2 family and candidate mediator of p53-induced apoptosis. *Science.* 288:1053–1058. https://doi.org/10.1126/science.288.5468.1053

Petroski, M.D., and R.J. Deshaies. 2005. Function and regulation of cullinRING ubiquitin ligases. *Nat. Rev. Mol. Cell Biol.* 6:9–20. https://doi.org/ 10.1038/nrm1547

Prudent, J., and H.M. McBride. 2017. The mitochondria-endoplasmic reticulum contact sites: a signalling platform for cell death. *Curr. Opin. Cell Biol.* 47:52–63. https://doi.org/10.1016/j.ceb.2017.03.007

Puthalakath, H., L.A. O'Reilly, P. Gunn, L. Lee, P.N. Kelly, N.D. Huntington, P.D. Hughes, E.M. Michalak, J. McKimm-Breschkin, N. Motoyama, et al. 2007. ER stress triggers apoptosis by activating BH3-only protein Bim. *Cell.* 129:1337–1349. https://doi.org/10.1016/j.cell.2007.04.027

Real, P.J., C. Sanz, O. Gutierrez, C. Pipaon, A.M. Zubiaga, and J.L. Fernandez-Luna. 2006. Transcriptional activation of the proapoptotic bik gene by E2F proteins in cancer cells. *FEBS Lett.* 580:5905–5909. https://doi.org/ 10.1016/j.febslet.2006.08.088

Rodriguez, D., D. Rojas-Rivera, and C. Hetz. 2011. Integrating stress signals at the endoplasmic reticulum: The BCL-2 protein family rheostat. *Biochim. Biophys. Acta.* 1813:564–574. https://doi.org/10.1016/j.bbamcr.2010.11 .012

Ruggiano, A., O. Foresti, and P. Carvalho. 2014. Quality control: ER-associated degradation: protein quality control and beyond. *J. Cell Biol.* 204: 869–879. https://doi.org/10.1083/jcb.201312042

Sanches, M., N.M. Duffy, M. Talukdar, N. Thevakumaran, D. Chiovitti, M.D. Canny, K. Lee, I. Kurinov, D. Uehling, R. Al-awar, et al. 2014. Structure and mechanism of action of the hydroxy-aryl-aldehyde class of IRE1 endoribonuclease inhibitors. *Nat. Commun.* 5:4202. https://doi.org/10 .1038/ncomms5202

Sartori da Silva, M.A., J.M. Tee, J. Paridaen, A. Brouwers, V. Runtuwene, D. Zivkovic, S.H. Diks, D. Guardavaccaro, and M.P. Peppelenbosch. 2010. Essential role for the d-Asb11 cul5 Box domain for proper notch signaling and neural cell fate decisions in vivo. *PLoS One.* 5:e14023. https:// doi.org/10.1371/journal.pone.0014023

Sher, Y.P., T.F. Tzeng, S.F. Kan, J. Hsu, X. Xie, Z. Han, W.C. Lin, L.Y. Li, and M.C. Hung. 2009. Cancer targeted gene therapy of BikDD inhibits orthotopic lung cancer growth and improves long-term survival. *Oncogene.* 28:3286–3295. https://doi.org/10.1038/onc.2009.187

Sher, Y.P., S.J. Liu, C.M. Chang, S.P. Lien, C.H. Chen, Z. Han, L.Y. Li, J.S. Chen, C.W. Wu, and M.C. Hung. 2011. Cancer-targeted BikDD gene therapy elicits protective antitumor immunity against lung cancer. *Mol. Cancer Ther.* 10:637–647. https://doi.org/10.1158/1535-7163.MCT -10-0827

Wan, L., M. Tan, J. Yang, H. Inuzuka, X. Dai, T. Wu, J. Liu, S. Shaik, G. Chen, J. Deng, et al. 2014. APC(Cdc20) suppresses apoptosis through targeting Bim for ubiquitination and destruction. *Dev. Cell.* 29:377–391. https://doi .org/10.1016/j.devcel.2014.04.022

Wang, Y., Z. Luo, Y. Pan, W. Wang, X. Zhou, L.S. Jeong, Y. Chu, J. Liu, and L. Jia. 2015. Targeting protein neddylation with an NEDD8-activating enzyme inhibitor MLN4924 induced apoptosis or senescence in human lymphoma cells. *Cancer Biol. Ther.* 16:420–429. https://doi.org/10 .1080/15384047.2014.1003003

Willis, S.N., J.I. Fletcher, T. Kaufmann, M.F. van Delft, L. Chen, P.E. Czabotar, H. Ierino, E.F. Lee, W.D. Fairlie, P. Bouillet, et al. 2007. Apoptosis initiated when BH3 ligands engage multiple Bcl-2 homologs, not Bax or Bak. *Science.* 315:856–859. https://doi.org/10.1126/science.1133289

Wu, H.C., Y.C. Lin, C.H. Liu, H.C. Chung, Y.T. Wang, Y.W. Lin, H.I. Ma, P.H. Tu, S.E. Lawler, and R.H. Chen. 2014. USP11 regulates PML stability to control Notch-induced malignancy in brain tumours. *Nat. Commun.* 5: 3214. https://doi.org/10.1038/ncomms4214

Xie, X., Y. Kong, H. Tang, L. Yang, J.L. Hsu, and M.C. Hung. 2014. Targeted BikDD expression kills androgen-dependent and castration-resistant prostate cancer cells. *Mol. Cancer Ther.* 13:1813–1825. https://doi.org/10 .1158/1535-7163.MCT-13-1004

Yamamoto, K., H. Yoshida, K. Kokame, R.J. Kaufman, and K. Mori. 2004. Differential contributions of ATF6 and XBP1 to the activation of endoplasmic reticulum stress-responsive cis-acting elements ERSE, UPRE and ERSE-II. *J. Biochem.* 136:343–350. https://doi.org/10.1093/jb/ mvh122

Ye, Y., H.H. Meyer, and T.A. Rapoport. 2001. The AAA ATPase Cdc48/p97 and its partners transport proteins from the ER into the cytosol. *Nature.* 414: 652–656. https://doi.org/10.1038/414652a

Ye, Y., W.K. Tang, T. Zhang, and D. Xia. 2017. A Mighty "Protein Extractor" of the Cell: Structure and Function of the p97/CDC48 ATPase. *Front. Mol. Biosci.* 4:39. https://doi.org/10.3389/fmolb.2017.00039

Yuan, W.C., Y.R. Lee, S.F. Huang, Y.M. Lin, T.Y. Chen, H.C. Chung, C.H. Tsai, H.Y. Chen, C.T. Chiang, C.K. Lai, et al. 2011. A Cullin3-KLHL20 Ubiquitin ligase-dependent pathway targets PML to potentiate HIF-1 signaling and prostate cancer progression. *Cancer Cell.* 20:214–228. https:// doi.org/10.1016/j.ccr.2011.07.008

Zhu, H., L. Zhang, F. Dong, W. Guo, S. Wu, F. Teraishi, J.J. Davis, P.J. Chiao, and B. Fang. 2005. Bik/NBK accumulation correlates with apoptosis-induction by bortezomib (PS-341, Velcade) and other proteasome inhibitors. *Oncogene.* 24:4993–4999. https://doi.org/10.1038/sj.onc .1208683